The Copernicus Sentinel-6 mission: Enhanced continuity of satellite sea level measurements from space

Craig J Donlon, Robert Cullen, Luisella Giulicchi, Pierrik Vuilleumier, C. Richard Francis, Mieke Kuschnerus, William Simpson, Abderrazak Bouridah, Mauro Caleno, Roberta Bertoni, et al.

The Copernicus Sentinel-6 mission: Enhanced continuity of satellite sea level measurements from space

Craig J. Donlon [a,*], Robert Cullen [a], Luisella Giulicchi [a], Pierrik Vuilleumier [a],
C. Richard Francis [a], Mieke Kuschnerus [a,e], William Simpson [a], Abderrazak Bouridah [a],
Mauro Caleno [a], Roberta Bertoni [a], Jesus Rancaño [a], Eric Pourier [a], Andrew Hyslop [g],
James Mulcahy [a], Robert Knockaert [a], Christopher Hunter [a], Alan Webb [a], Marco Fornari [h],
Parag Vaze [b], Shannon Brown [b], Joshua Willis [b], Shailen Desai [b], Jean-Damien Desjonqueres [b],
Remko Scharroo [c], Cristina Martin-Puig [c], Eric Leuliette [d], Alejandro Egido [d], Walter H.F. Smith [d],
Pascal Bonnefond [f], Sophie Le Gac [i], Nicolas Picot [i], Gilles Tavernier [i]

[a] European Space Agency ESA/ESTEC, Keplerlaan 1, 2201, AZ, Noordwijk, the Netherlands
[b] Jet Propulsion Laboratory, California Institute of Technology, Pasadena, CA, USA
[c] EUMETSAT, Darmstadt, Germany
[d] NOAA Center for Satellite Applications and Research, MD, USA
[e] Now at TUD, Delft, the Netherlands
[f] SYRTE, Observatoire de Paris, PSL Research University, CNRS, Sorbonne Universités, UPMC, Univ. Paris 06, LNE, 77 Avenue Denfert-Rochereau, 75014 Paris, France
[g] Vitrociset, a Leonardo Company, for ESA, Huygensstraat, 2201 DK Noordwijk, The Netherlands
[h] RHEA for ESA, Noordwijk, the Netherlands
[i] CNES, Toulouse, France

ARTICLE INFO

ABSTRACT

Given the considerable range of applications within the European Union Copernicus system, sustained satellite altimetry missions are required to address operational, science and societal needs. This article describes the Copernicus Sentinel-6 mission that is designed to provide precision sea level, sea surface height, significant wave height, inland water heights and other products tailored to operational services in the ocean, climate, atmospheric and land Copernicus Services. Sentinel-6 provides enhanced continuity to the very stable time series of mean sea level measurements and ocean sea state started in 1992 by the TOPEX/Poseidon mission and follow-on Jason-1, Jason-2 and Jason-3 satellite missions. The mission is implemented through a unique international partnership with contributions from NASA, NOAA, ESA, EUMETSAT, and the European Union (EU). It includes two satellites that will fly sequentially (separated in time by 5 years). The first satellite, named Sentinel-6 Michael Freilich, launched from Vandenburg Air Force Base, USA on 21st November 2020. The satellite and payload elements are explained including required performance and their operation. The main payload is the Poseidon-4 dual frequency (C/Ku-band) nadir-pointing radar altimeter that uses an innovative interleaved mode. This enables radar data processing on two parallel chains the first provides synthetic aperture radar (SAR) processing in Ku-band to improve the received altimeter echoes through better along-track sampling and reduced measurement noise; the second provides a Low Resolution Mode that is fully backward-compatible with the historical reference altimetry measurements, allowing a complete inter-calibration between the state-of-the-art data and the historical record. A three-channel Advanced Microwave Radiometer for Climate (AMR—C) provides measurements of atmospheric water vapour to mitigate degradation of the radar altimeter measurements. The main data products are explained and preliminary in-orbit Poseidon-4 altimeter data performance data are presented that demonstrate the altimeter to be performing within expectations.

1. Introduction and background to the Sentinel-6 mission

Satellite altimetry is a fundamental tool for the European Copernicus services providing measurements over the global ocean and, increasingly in the coastal zones and inland waters. Microwave radiometers supporting radar altimeter payloads are also extensively used to monitor atmospheric characteristics in the troposphere (e.g. Varma et al., 2020; Quilfen and Chapron, 2019; Quartly et al., 2000). The importance of satellite altimetry cannot be overstated in terms of the impact on operational oceanography (e.g. Munk, 2002; Le Traon et al., 2019) and climate science (e.g. IPCC, 2014, 2019). Measurements are used in a variety of applications to enable quasi-global estimates of sea level rise (e.g. Cazenave et al., 2018; Veng and Andersen, 2020; Ablain et al., 2015), ocean sea state (e.g. Ardhuin et al., 2019; Ribal and Young, 2019; Dodet et al., 2020), large-scale ocean and mesoscale circulation, (~30–300 km and ~ 5–90 day) (e.g. Chelton et al., 2007), wind speed over the ocean (e.g. Abdalla, 2012; Bushair and Gairola, 2019), estimates of sea ice thickness and volume (e.g. Tilling et al., 2018), geodesy applications (e.g. Bloßfeld et al., 2020) and ionospheric mapping (e.g. Ray, 2020). Satellite altimetry increasingly contributes to our understanding of the hydrological cycle by monitor variations in the height and extent of rivers, lakes, reservoirs and flooded regions (e.g. Emery et al., 2018; Gao et al., 2019; Roohi et al., 2019). In Copernicus (EU, 2014), measurements are used for operational ocean monitoring/forecasting and derivation of geostrophic ocean currents by the Copernicus Marine Environment Monitoring Service (CMEMS, e.g. Le Traon et al., 2015, 2019), wave forecasting and climatology (e.g. Campos et al., 2020; Bidlot, 2017; Cooper and Forristall, 1997), climate monitoring/prediction by the Copernicus Climate Change Service (C3S, Buontempo et al., 2020), numerical weather prediction (e.g. Campos et al., 2020), the study of ocean tides (e.g. Carrere et al., 2020) and gravity field mapping (Sandwell et al., 2019). Other diverse applications include seafloor mapping (Smith and Sandwell, 1997), investigation of ocean wave-current interaction (Quilfen and Chapron, 2019), dual-frequency radar altimeter inputs to computation of rain rates (Quartly et al., 1999, 2000), computation of ocean/atmosphere gas fluxes (e.g. Frew et al., 2007; Goddijn-Murphy et al., 2013), monitoring ship traffic (Tournadre, 2014), estimating extreme waves (e.g., Alves and Young, 2004; Hanafin and Coauthors, 2012), tracking icebergs (Tournadre et al., 2008). Given the considerable range of applications, sustained altimetry satellite missions are required to address operational science and societal needs.

The Sentinel-6 mission has a specific focus on sea level rise measurements and sea state measurements. The successful implementation of long lead time adaptation measures to sea level rise are particularly important for Copernicus stakeholders. The trend of sea level rise is required to validate model projections, separate internal from forced variability and determine which areas are prone to coastal flooding (Hamlington et al., 2020). The International Panel for Climate Change (IPCC, 2019) note that the total mean sea level rise for 1902–2015 is 0.12–0.21 m. The rate of rise for 2006–2015 is 3.1–4.1 mm yr^{-1} which is much larger than the 1901–1990 rate of 0.8–2.0 mm yr^{-1}. The predicted rise in mean sea level is strongly dependent on the IPCC Representative Concentration Pathway (RCP) emission scenario that is followed with estimates of 0.29–0.59 m (RCP2.6) and 0.61–1.10 m (RCP8.5) by 2100 relative to 1986–2005. By the end of the century, sea level rise is projected to be faster under all IPCC scenarios, including those compatible with achieving the long-term temperature goal set out in the Paris Agreement (e.g. Garbe et al., 2020).

Such an acceleration of sea level rise is dramatic (e.g. Chen et al., 2017; Cazenave et al., 2018) and poses a significant threat to populations living in low-lying coastal regions and small islands (IPCC, 2019). Sea level rise acceleration derived from satellite altimetry has been estimated by several authors (e.g. Dieng et al., 2017; Nerem et al., 2018; Veng and Andersen, 2020). Since January 1993, the majority of recent estimates suggest that the mean sea level is rising at a mean rate of 3.2 ± 0.3 mm yr^{-1} (e.g. Quartly et al., 2017, WCRP, 2018 and Fig. 1). At the regional scale, ocean thermal expansion is the main cause of the spatial trend patterns observed by satellite altimetry (e.g. Cazenave et al., 2018) and the loss of ice from the Greenland and Antarctic ice sheets and from terrestrial glaciers is now the main contributor to sea level rise (e.g. IPCC, 2019). Since 1970, the global ocean has absorbed more than 90% of the excess heat in the climate system (IPCC, 2019) and since 1993, the rate of ocean warming has increased. A record was reached in 2020 (Cheng et al., 2021) with measured impacts on the ocean heat content to at least 2000 m (there are very few measurements below 2000 m available to determine impacts below this depth). The associated ocean thermal expansion (steric) global mean sea-level change of ocean warming is estimated as 1.36 ± 0.10 mm yr^{-1} for 1993–2017 from a combination of different noise models that provide variability and uncertainty estimates (Camargo et al., 2020).

Since 1992 four satellite radar altimeter missions have provided a sustained 'reference' altimetry capability occupying the same 'reference' orbit (±66.04° inclination, 1339–1356 km altitude, 112 min per revolution) providing a 9.9-day repeat track orbit. These are TOPEX/Poseidon (T/P) (launched in August 1992, e.g. Fu et al., 1994), Jason-1 (launched in December 2001, e.g. (Ménard and Fu, 2001), OSTM/Jason-2 (launched in June 2008, e.g. (NASA, 2011), and Jason-3 (launched in January 2016) described by Lambin et al. (2010) and Vaze et al. (2010). Each satellite has been launched sequentially to provide measurements to which all other altimeters are adjusted (e.g. Legeais et al., 2018; Ducet
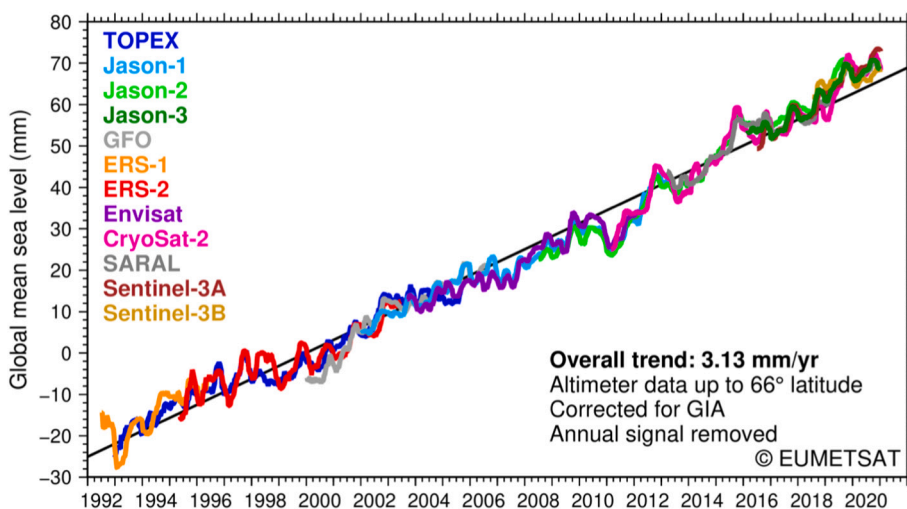
Fig. 1. Mean Sea level estimates computed from different satellite altimeter records maintained in the RADS data base (Scharroo et al., 2013) from 1992 to 2020. Seasonal signals have been removed and the data are corrected for Glacial Isostatic Adjustment (GIA). TOPEX data are corrected following Beckley et al. (2017) and no long-wavelength, trend, or acceleration adjustments have been made. Large variations are observed around the multi-mission linear trend, due to large-scale ocean signals, planetary mass redistribution, and interannual variability. Strong variations exist in regional estimates of the mean sea level variation. Continuous improvement in altimeter system sampling, performance and data product accuracy, for all components of the system (altimeter and radiometer sensors, orbit calculation and geophysical corrections) is required to enhance confidence in the application of these measurements.

et al., 2000) including high orbit inclination missions such as CryoSat-2 (Wingham et al., 2006), and polar orbiting mission such as SARAL/ AltiKa, (Steunou et al., 2015) and Copernicus Sentinel-3 ((Donlon, 2011) Donlon et al., 2012). This is important, since the small measurement footprint of nadir viewing altimeters (between ~2 to ~15 km depending on sea state and radar frequency) severely limits sampling of the ocean both in time and in space and that multiple missions must be used together. A notable challenge for the 'Next Generation' of Copernicus altimeters is to significantly improve the sampling to ~50 km and ~5 days to meet the needs of high resolution (1/36°) global ocean models (Le Traon et al., 2019). The reference orbit was chosen to limit the impact of tidal signals (e.g. Parke et al., 1987) that must be removed from satellite altimetry data that includes several components of known frequencies (e.g. Huess and Andersen, 2001; Łyszkowicz and Bernatowicz, 2017). Sentinel-6 inherits this orbit choice which is maintained to assure the long-term stability of the sea level record from space (e.g. Ablain et al., 2019) and the long-term stability of measurements (a fundamental user requirement for Sentinel-6).

Fig. 1 shows a multi-mission time series of altimeter sea level rise based on the work of Scharroo et al. (2013). Complications arise when deriving rate trends due to the known drift in the Topex-A mission (e.g. Dieng et al., 2017; Ablain et al., 2019; Nerem et al., 2018) which have been included in this figure. However, Hamlington et al. (2020) note that the altimeter record is too short to draw conclusive evidence on regional acceleration trends due to the detrimental impact of natural variability in known climate modes (e.g. Pacific decadal oscillation, El Niño) on trend analysis. If these are accounted for, regional estimates of sea level acceleration are significantly dampened.

In addition to sea level rise, satellite altimetry provides the most comprehensive and longest globally sampled record of sea state available today. Significant Wave Height (Hs) estimates (e.g. Ardhuin et al., 2019) are a fundamental input to derive accurate sea-level estimates since the impact biases associated with sea state uncertainty (2 cm) remain the largest contributor to a satellite altimeter range measurement (Table 1). The impact of sea level rise is considerably enhanced at moderate to high sea states in coastal regions and low-lying islands. The

IPCC (2019) notes that extreme wave heights, have increased in the Southern and North Atlantic Oceans by around ~0.8 cm yr^{-1} over the period 1985–2018. Within Copernicus, applications relating to maritime safety led by the European Maritime Safety Agency (EMSA) together with operational oceanography led by CMEMS, require Hs measurements for wave modelling activities (e.g. Le Traon et al., 2019; Lorente et al., 2018). Hs is also used to monitor and improve models of extreme events including hurricane intensification (e.g. Scharroo et al., 2005), storm surge (e.g. Madsen et al., 2015), and tsunamis (e.g. Smith et al., 2005; Ablain et al., 2006) among others. Sea-state has a significant role in climate applications because it modifies the exchange of heat, mass, momentum and gas between the ocean and atmosphere (e.g. Leighton et al., 2018) that plays a significant role in the global cycles of energy, water and carbon. New efforts are in progress (e.g. Dodet et al., 2020) to homogenize satellite altimeter Hs data sets from different missions and provide a stable, well calibrated and quality-controlled sea state record as a contribution to the Global Climate Observing System (GCOS, 2016) Essential Climate Variables ECV (GCOS, 2011; NRC, 2004). Satellite measurements are of particular value in the southern hemisphere, and in some poorly sampled regions of the northern hemisphere, where climate trend determination is complicated by the limited in situ data available.

To ensure decision makers and policy makers have timely and easy access to the best information on aspects of societal relevance, including sea level rise, the European flagship Copernicus Earth Observation programme has been established (EU, 2014) to provide environmental information to understand how our planet and its climate are changing, the role of human activities in these changes and how these will influence our daily lives. Led by the European Union (EU) with the European Space Agency (ESA) managing the space component, Copernicus is setting worldwide standards. Copernicus is founded on dedicated Services (e.g. Matevosyan et al., 2017) including CMEMS, C3S and the Copernicus Global Land Monitoring Service (CGLMS) that depend on the provision of satellite altimetry in an operational context. The Sentinel-6 mission is a direct response to user needs expressed by the Copernicus Programme and internationally (Escudier and Fellous, 2008). The first satellite has been named Sentinel-6 'Michael Freilich' (S6-MF) in recognition of the outstanding contribution to Earth Observation of Dr. Freilich, former director of NASA's Earth Science Division. It is primarily designed to measure global sea level change and variability (e.g. WCRP, 2018) by ensuring continuity and extended capability of satellite altimetry "reference" measurements (i.e. Sea Surface Height (SSH), Significant Wave Height (Hs) and wind speed) without degradation in precision or accuracy Couderc (2015).

As Copernicus regional models develop (e.g. Ponte et al., 2019), there is a strong demand for improved altimeter measurement accuracy and sampling in the coastal regions (e.g. Vignudelli et al., 2011; Le Traon et al., 2019; Climate Change Initiative Coastal Sea Level Team, 2020). This is a challenge due to the relatively large antenna footprint of radar altimeters and supporting microwave radiometers that inevitably sample both ocean and land surfaces in the coastal zone. Building on the demonstrated capability of the ESA CryoSat 2 Mission (Wingham et al., 2006; Francis, 2002), the Copernicus Sentinel-3 mission (e.g. Donlon et al., 2012) included a synthetic aperture radar (SAR) altimeter employing delay/Doppler techniques (Raney, 1998, Francis, 2002, Le Roy et al., 2010) to improve altimeter measurements (e.g. Gommenginger et al., 2013a, Gommenginger et al., 2013b) and in the coastal regions (Gommenginger et al., 2012, Passaro et al., 2014) although this mission now operates in SAR mode globally. Over the open ocean these have demonstrated that SAR mode altimetry brings a significant improvement due to the increased number of radar looks (and reduction in random noise) at a given Earth location (e.g. Boy et al., 2016; Clerc et al., 2020). Furthermore, SAR altimetry is particularly beneficial over river and lake targets (e.g. Taburet et al., 2020). Based on this heritage, an improved SAR altimeter is included in the S6-MF mission.

This paper provides a review of the Copernicus Sentinel-6 mission that responds directly to Copernicus user needs. Within Copernicus, to

Table 1

Sentinel-6 Mission Performance Requirements from Scharroo (2018) specified at Hs = 2 m, sigma0 = 11 dB and 1 Hz. (NRT = Near Real Time within 3 h of data acquisition, STC=Short-Time Critical within 36 h of data acquisition, NTC = Non Time Critical within 60 days of data acquisition).

Parameter	Requirements (NRT/STC/ NTC)	Goal (NRT/STC/ NTC)
Ku-band range noise[a]: Low Resolution (cm)	1.5	1.0
Ku-band range noise[a]: High Resolution (cm)	0.8	0.5
Ionosphere[b] (cm)	0.5	0.3
Sea state bias (cm)	2.0	1.0[e]
Dry troposphere (cm)	0.8/0.7/07	0.5
Wet troposphere (cm)	1.2/1.2/1.0	0.8
Goal RMS ellipsoid-normal (radial) orbit (cm)	5.0/2.0/1.5	3.0/1.5/1.0
Total RSS SSH: Low resolution (cm)	5.79/3.53/3.20	4.2/3.5
Total RSS SSH: High resolution (cm)	5.65/3.29/2.94	3.53/2.12/1.80
Hs[c] (0.5–20 m)	15 cm ±5%	10 cm ±5%
Wind speed (for 3 to 20 m s^{-1})	1.5 m s^{-1}	1.0 m s^{-1}
σ⁰ (-10 dB - +50 dB)[d]	0.3 dB	0.3 dB

a. After ground processing, averaged over 1 s, for 2 m wave height.
b. Derived from Ku- and C-band range difference, averaged over 200 km.
c. Valid for the range of 0.5 to 8 m Hs.
d. After cross-calibration with other altimeter missions.
e. Could also be expressed as 1% of Hs, to be reached at the end of the commissioning phase.

address sampling requirements for operational ocean forecasting, the twin-satellite polar-orbiting Sentinel-3 (e.g. Donlon et al., 2012) and the Sentinel-6 reference missions will work together as a Copernicus altimetry constellation. In the following sections, the satellite configuration and payload complement is described and the data products from the mission summarised. Finally, we conclude with an assessment of early in-orbit performance for the first Sentinel-6 satellite successfully launched on 21st November 2020.

2. Sentinel 6 mission configuration

Formal end user requirements for the Sentinel-6 mission have been established and agreed by the Sentinel-6 Partners and are documented in Scharroo (2018). Table 1 sets out the primary mission performance requirements and we highlight that uncertainties for sea level observations must be equivalent or better than those of the heritage Jason missions (e.g. CNES, 2006, 2011).

Sentinel-6 includes two identical satellites that will be launched sequentially (with an expected ~5 year launch separation) into the altimetry reference orbit with S6-MF overlapping with Jason-3 (Sentinel-6B will then overlap with S6-MF after launch). The nominal operational lifetime of each satellite is 5.5 years including commissioning, although sufficient consumables are included to extend the mission lifetime up to 2 more years as an extended operations phase (in agreement with the European Commission) before active deorbit. Fig. 2 presents a summary overview of the Sentinel-6 system.

The payload for each Sentinel-6 satellite includes:

1. A dual-frequency Ku/C-band nadir-pointing radar altimeter with Ku-band operating as a synthetic aperture radar (Poseidon-4),
2. A multifrequency Advanced Microwave Radiometer for Climate (AMR—C) including an experimental High-Resolution Microwave Radiometer (HRMR),
3. A Precise Orbit Determination (POD) suite comprising Global Navigation Satellite System (GNSS) receivers, a Laser Retroreflector Array (LRA) and a Doppler Orbitography Radio-positioning Integrated by Satellite (DORIS) system,
4. As a secondary payload, a GNSS Radio Occultation (GNSS-RO) sensor,

5. A Radiation Environment Monitor (REM) sensor.

Each of these elements is discussed in dedicated sections below.

3. Sentinel-6 satellite

The satellite configuration is derived from ESA's CryoSat (Francis, 2002; Wingham et al., 2006). That mission had many of the same drivers as Sentinel-6 including flying in a non-sun-synchronous orbit and the

Table 2
General overview of the Sentinel-6 satellite applicable to Michael Freilich and Sentinel-6B.

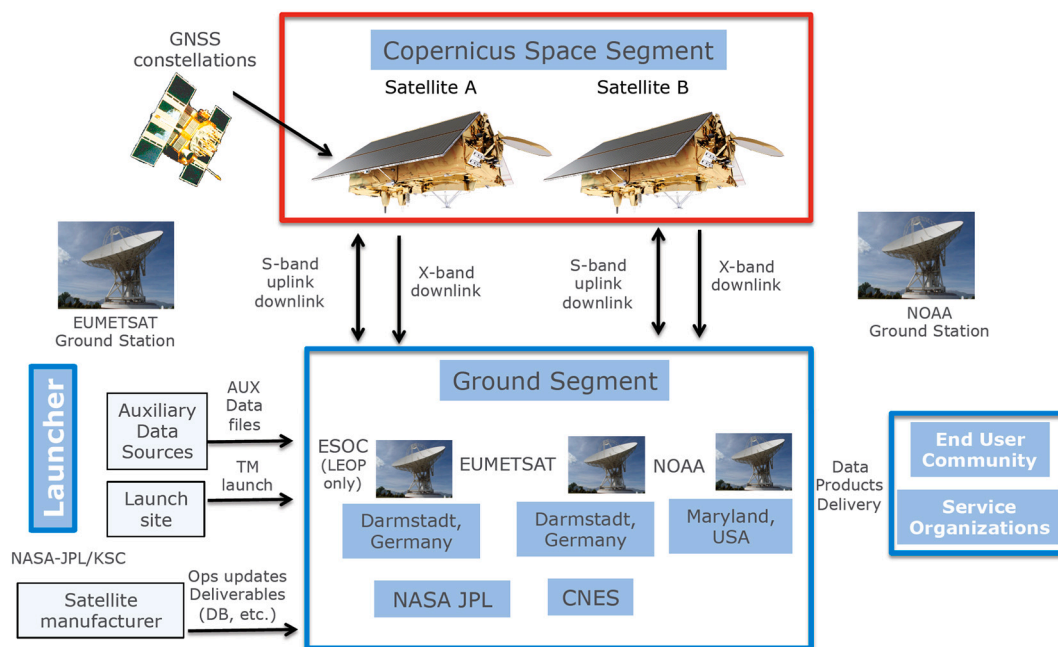|	
Orbit	Low Earth Orbit, non sun-synchronous ● Repeat cycle: 9.92 days ● Mean altitude: 1336 km; Inclination: 66° providing coverage of the Earth surface between 66° north and south of the equator.
Lifetime	5-year operational mission (with consumables for an additional 2 years) and 6 months for commissioning activities.
Satellite	● Platform derived from ESA's CryoSat Mission ● Flight configuration 5.13 m × 4.33 m × 2.35 m ● Stowed configuration 5.13 m × 2.58 m × 2.35 m ● Mass: 1191 kg including 230 kg fuel (225 kg after LEOP) ● Power: 891 W average consumption ● Data: Volume: order of magnitude 1200 Gbit/day; On-board storage: 576Gbit ● Communications: X-band data downlink: 150 Mbps at 8.090 GHz (ESA) S-band Telemetry Tracking and Comand (TTC) link: 16 kbps uplink, 32 kbps for 1 Mbps downlink
Instruments	● Dual-frequency Radar Altimeter: Poseidon-4 (ESA) ● Advanced Microwave Radiometer for Climate (AMR—C) including High Resolution Microwave Radiometer (HRMR, NASA/JPL) ● Precise Orbit Determination: GNSS POD Receiver, DORIS (ESA) ● Laser Retroreflector Array (NASA/JPL) ● GNSS-RO TriG Receiver for Radio Occultation (NASA/JPL) ● Radiation Environment Monitor (ESA)
Flight Operations	Mission control for Launch and Early Operations Phase (LEOP) from ESA Satellite Operations Centre (ESOC). In orbit verification, Commissioning and routine operations from EUMETSAT. Two operational ground stations, at Fairbanks (NOAA) and Kiruna (ESA).
Launch Vehicle	Falcon-9 (NASA-JPL/KSC).

Fig. 2. Sentinel-6 System overview.

need to optimise the configuration towards the precise determination of its orbit. Table 2 provides a summary overview of the main satellite characteristics. Unlike its predecessors Jason 1, 2 and 3, the satellite features body mounted solar arrays which means that both the variable drag cross section caused by moving solar arrays and the necessary rotation of the satellite body about the yaw axis are avoided. The satellite also minimises the presented area in the direction of flight to minimise the impact of drag. These design features result in a stable satellite platform.

An accurate knowledge of the altimeter antenna phase-centre with respect to the reference ellipsoid is paramount to precisely derive the SSH from the range measured by the altimeter radar. This implies accurate knowledge of the satellite orbit and its system Centre of Mass (CoM) throughout the mission lifetime. The major source of moving mass within the spacecraft is the propellant within the fuel tank (~20% of total spacecraft mass). A specially developed tank baffle system has been implemented that enables the determination of the fuel distribution within the tank as it is depleted. The satellite CoM knowledge is 0.33 mm in the direction parallel to the altimeter boresight over the mission lifetime. The spacecraft is fuelled with 230 kg hydrazine monopropellant of which 62% is used for active de-orbit mission disposal, the remaining fuel is used to acquire the orbit and perform a tandem flight (Donlon et al., 2019) with Jason-3 (~12%) and nominal operations.

Since the orbit is non-synchronous with a drifting orbit plan and varying solar aspect angle, the satellite is designed with a roof shaped solar array ($15m^2$ GaAs triple junction cells with 30% efficiency). This maximises solar power over the lifetime without the need to steer the arrays in a similar manner to Jason 1/2/3. A lithium ion (Li-Ion) battery stores sufficient energy to power the satellite system with its payload complement during eclipses and in case of contingency over the mission lifetime. Fig. 3 shows several views of S6-MF.

GNSS antennas are located on the roof of the satellite to optimise reception of both Global Positioning System (GPS) and Galileo constellation signals. A large Earth-facing panel hosts the Poseidon-4 altimeter, the LRA, the DORIS antenna and communications antennas. Satellite command and control are implemented via a bi-directional S-band communication link. Scientific data collected over each orbit are stored in 576 Gb solid-state mass memory prior to downlink to the ground station (via X-band link) at a data rate of 150 Mbps (sufficient to downlink one full orbit of data using a single ground station overflight). Accurate altimeter pulse-to-pulse datation ($<$ 5 microseconds) is essential for the Sentinel-6 mission because datation errors transform into range measurements errors via the variations in the orbit height rate of change (which can exceed 25 m s^{-1}). This requires a very accurate on-board clock (provided by a new miniaturised DORIS Ultra Stable Oscillator, RK410 mini-USO) and time synchronisation across the spacecraft sub-systems. For this purpose, the on-board computer distributes a hardware pulse every second as time reference for all equipment which is synchronised to atomic time whole seconds when the on-board GNSS receiver is tracking.

The spacecraft equipment is designed to operate within a relatively narrow thermal range (typically 273-313 K). In order to maintain this temperature range, the heat generated by the satellite payload and systems in operation must be emitted by arranging radiating surfaces that ideally, always point to cold space. With the non-sun-synchronous orbit of Sentinel-6 there is no face that is always pointing to deep space. While a small radiator panel located on the top of the satellite is provided, following the CryoSat heritage, Sentinel-6 makes use of the large nadir facing panel that always points to the Earth. While not as cold as deep space, this view is relatively stable although a larger radiator area is required to meet thermal requirements.

The AOCS and Reaction Control System (RCS, including gyroscope, Coarse Earth and Sun Sensors (CESS), and a magnetometer) maintain satellite attitude pointing control. The expected pointing accuracy is $\pm0.11°$ (3-σ), knowledge of $\pm0.055°$ and stability of ~700 microdegrees

over a window of 0.5 s. After separation near the operational orbit, the spacecraft angular rate is damped using the thrusters, then the solar panels are deployed with the attitude control idled. Subsequently the attitude is maintained in a coarse 3-axis nadir pointing using a combination of thrusters and magnetorquers. Fine three-axis stabilization used during science acquisitions is acquired using the star tracker in conjunction with the GNSS receiver to point the altimeter line of sight to the local nadir and compensate the Earth rotation by yaw steering. The reaction wheels are used as actuators and are continuously off-loaded using magneto-torquers. Orbit corrections are performed in a dedicated orbit control mode (OCM) where the thrusters fire almost continuously to provide required delta-velocity increment. The OCM was used early in the mission to gradually raise the launcher injection orbit up to the operational orbit and rendez-vous with Jason-3 and form a tandem flight convoy formation. The OCM is also used routinely to maintain the spacecraft ground track within ±1 km of the reference ground track and, at the end of the mission, to lower the orbit perigee allowing the orbit to decay and the satellite to re-enter the Earth atmosphere within 25 years.

4. Sentinel-6 poseidon-4 altimeter

Poseidon-4 is a nadir-pointing dual-C/Ku-band frequency synthetic aperture radar altimeter (only the Ku-band operates in SAR) designed to provide high accuracy and high precision altimetry measurements including SSH derived from the radar range, and sea state and wind speed from normalised radar cross section (σ^0). The SSH is provided as a height above the reference ellipsoid (WGS-84) computed from the difference of altimeter range (corrected from atmospheric and sea-state effects) and the satellite altitude (provided by POD system).

Poseidon-4 uses a 9 kHz Pulse Repetition Frequency (PRF) that is ~4 times greater than Jason-3. An interleaved radar chronogram is used to enable simultaneous operation of SAR and Low Resolution Mode (LRM) heritage acquisitions to ensure that the introduction of SAR technologies into the reference orbit does not introduce a bias into the long-term sea level climate record derived from LRM only measurements. The interleaved (open burst) transmit and receive approach means that twice the number of samples are available compared to the Copernicus Sentinel-3 radar altimeter (SRAL, LeRoy et al., 2009) bringing a notable improvement of altimeter noise characteristics.

TOPEX/Poseidon and Jason-1/2 all demonstrated the ability to accurately measure trends in global sea level but no formal design requirement on long-term drift was ever levied on these mission designs. Jason-3 included a design goal to measure globally averaged sea level relative to levels established during the cal/val phase with zero bias ±1 mm (standard error) averaged over any one year period (Lambin et al., 2011). For Sentinel-6, to enhance the sea level rise time series, formal measurement drift requirements that arise from different contributions impacting mean sea level were adopted as set out in Table 3.

Assuming that all recognised significant systematic effects are corrected and noting that for climate quality products, the combined standard uncertainty of the 1-s along-track averaged SSH measurements shall be less than 3.2 cm during the whole operational period (Table 1), a regional drift requirement of ~3.5 cm is implicit over the mission lifetime. We note that new analyses (e.g. WCRP, 2018; Ablain et al., 2019) and the assessments made in the ESA Climate Change Initiative (CCI) sea Level project, (Legeais et al., 2018) suggest that even stricter requirements are needed for future missions.

4.1. Poseidon-4 instrument description

The Poseidon-4 instrument uses a single nadir-pointing antenna externally mounted on the large nadir-facing panel of the satellite connected to a Digital Processing Unit (DPU) and Radio-Frequency Unit (RFU) mounted inside the satellite. Full redundancy of the electronic units is required to meet instrument reliability requirements over the
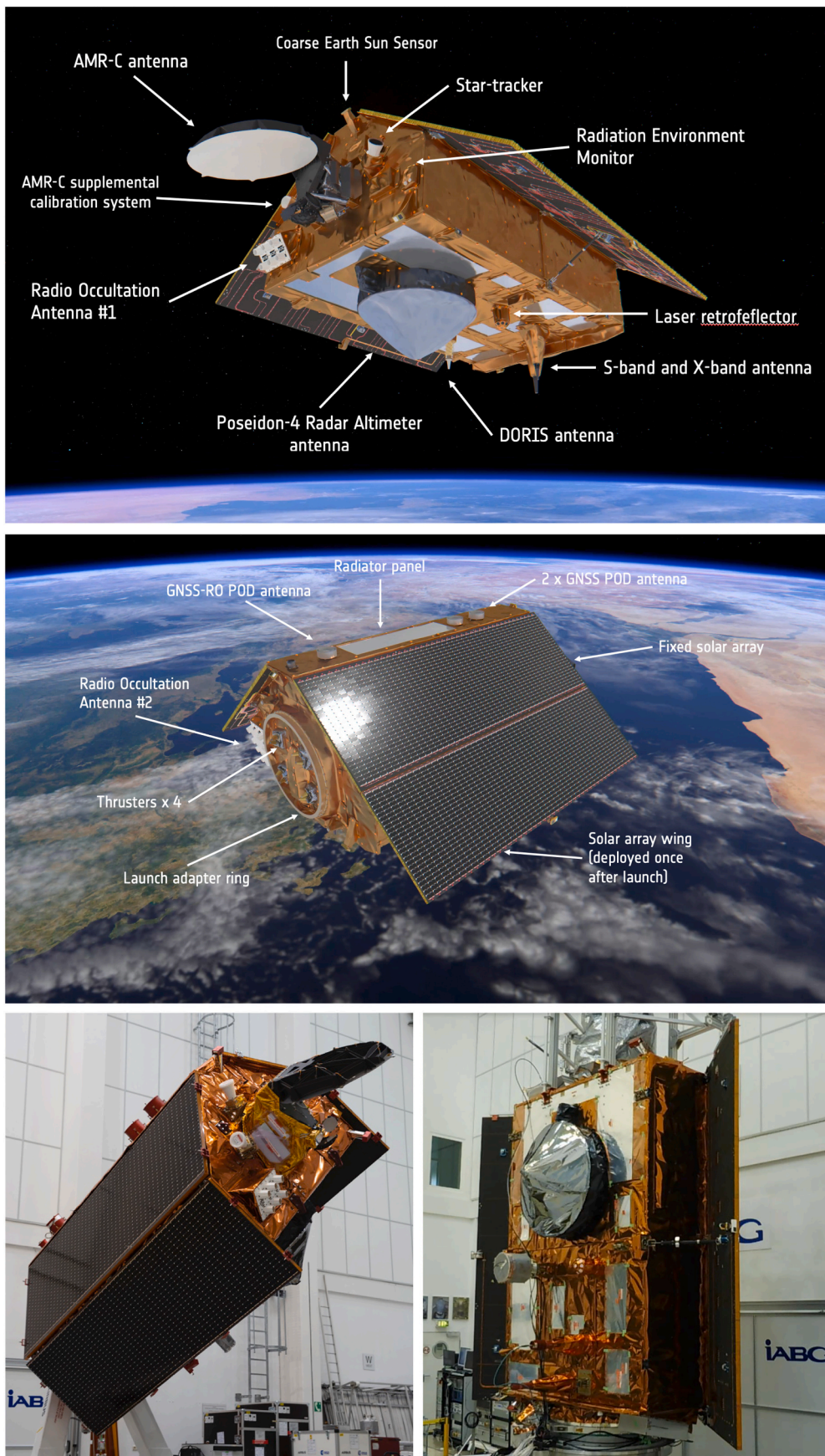
Fig. 3. (top (A) and middle (B)) Sentinel-6 Michael Freilich satellite and external features. (bottom) satellite during tests at IAGB facilities, Germany (C) with solar wings in stowed position and (D) after solar wing deployment test.The forward facing panel of the spacecraft hosts the AMR—C, Star-tracker heads, one GNSS-RO instrument antenna and the REM instrument. The AMR-C line-of-sight towards the Earth is arranged to ensure alignment of altimeter and radiometer footprints on ground. S6-MF uses star trackers to determine its absolute attitude in inertial space. Three star tracker heads point in different directions to prevent blinding of one or the other by sunlight or moonlight at some point in an orbit. In the event of a failure, the two remaining star tracker heads will be able to provide attitude measurements most of the time. Star-Trackers are also used within the on-board Attitude and Orbit Control System (AOCS), providing attitude information (quaternions) key to the Poseidon-4 SAR retrievals that are sensitive to platform 'mis-pointing' from the nominal local normal yaw steered. The quaternions provide key attitude information for POD processing. The GNSS-RO forward looking antenna array is inclined towards the Earth limb to track the GNSS satellite signals that rise or set at the horizon as they traverse the Earth atmosphere. A second array is accommodated on the aft external bulkhead panel to acquire occultation profiles from the opposite direction. The GNSS-RO also has a dedicated POD antenna mounted on the roof of the satellite that provides additional information for primary mission POD.

Table 3
Sentinel-6 measurement drift requirements.

Measurement	Drift Requirement (1 σ)	Note
Global mean sea level	1 mm yr^{-1}	Approximately 1/3 of the established value of global mean sea level rise over the altimeter era.
Altimeter range	0.7 mm yr^{-1}	
Orbit error	0.1 mm yr^{-1}	as a result of unmodelled or imperfectly modelled reference frame or gravity field variations
Microwave radiometer	0.7 mm yr^{-1}	
SSB (from backscatter coefficient)	0.1 mm yr^{-1}	due to drifts in backscatter
Geophysical corrections	0.1 mm yr^{-1}	
Regionally averaged sea level	5 mm yr^{-1}	average of all sea level measurements within one repeat cycle within an ocean area of approximately 40,000 km^2 (approximately 2° by 2°)

mission lifetime. This arrangement results in preferred short connections between the antenna, DPU and RFU while providing a clear view of the Earth surface. The RFU includes C-band and Ku-band power amplifiers with gain control, signal transmit, receive and signal routing functions. The Poseidon-4 DPU manages communication interfaces to the satellite platform, the high-bandwidth digital Ku-band chirp generator, instrument sequencing, processing of received echoes from the Earth surface, digital compression and tracking functions. The maximum bandwidth of the digital chirp is 320 MHz with a pulse duration 32 μs. The DORIS instrument provides a 10 MHz ultra-stable reference to generate the Poseidon-4 internal clock signal.

Fig. 4 shows a functional block diagram of the Poseidon-4 instrument. The antenna is a 1.2 m diameter single symmetrical parabolic reflector that is centre-fed with a dual frequency feed chain at a focal length of about 440 mm. The primary altimeter frequency is at Ku-band (central frequency: 13.575 GHz, total bandwidth: 320 MHz) with SAR capability. The secondary C-band frequency (central frequency: 5.41 GHz, total bandwidth: 320 MHz) LRM capability is used for ionospheric Path Delay (PD) correction to better than 0.7 cm, rain cell measurements and surface roughness estimates. Both C-band and Ku-band channels use linear polarization arranged so that the polarization vector of each channel is set orthogonal to each other. In addition, the C-band channel is set orthogonal to the polarization vector of the nominal AMR-C instrument to minimise interference. Radiometer blanking signals are provided by the altimeter to the AMR radiometer. Radio frequency contamination analysis at satellite level shows sufficient margins and blanking pulses are not expected to be used. If needed, the blanking pulses will be used by the radiometer to stop integrating measurements when the altimeter is emitting RF pulses in C-Band and/or in Ku-Band.

I and Q signals are digitally sampled from the received analogue chirp echoes obtained by the analogue receive chain after direct demodulation from the initial RF frequency. Digital pulse range compression transforms the received chirp using a matched filter at the PRF. These form a Brown-like LRM echo waveform (Brown, 1977) over the ocean surface (different echo shapes will be generated for other target surface types) with a range resolution of ~42 cm.[1] LRM measurements are derived using the conventional approach of power detection after range compression and incoherent averaging (nominally over a time window of 50 ms). LRM measurements are required by onboard acquisition and tracking algorithms and thus, are always available

in the altimeter data stream when the instrument is operating. SAR measurements at full resolution are extracted after range digital compression and can be downlinked over specific regions defined in a dedicated mode mask - although the data volume is large. As this is the case, on-board azimuth processing of 64 pulses is performed followed by range migration compensation and a truncation of the data (described later).

Fig. 5 shows the evolution of nadir altimeter radar chronogram used to acquire measurements for different satellite missions. The TOPEX/Poseidon and Jason heritage missions within the altimeter reference time series have all used LRM measurement strategies in which radar pulses are continuously transmitted and received at a pulse repetition frequency of ~2 kHz. The ESA CryoSat2 Earth Explorer SIRAL instrument (Francis, 2002) first employed a closed burst SAR mode altimeter in space for Earth observation purposes (Cullen et al., 2006) and pioneered SAR altimeter retrievals (e.g. Boy et al., 2016). Based on this successful demonstration, the Copernicus Sentinel-3 (Donlon, 2011) SAR radar ALtimeter (SRAL, Le Roy et al., 2010) was developed also using a closed burst measurement strategy based on a sequence of 64 transmit pulses. Fig. 5 highlights that in both cases, at least half the duty cycle time of the altimeter (a factor 4 for closed burst SAR depending on the burst rate and number of pulses per burst) is unused as the altimeter must wait for the echoes to be returned to the antenna.

To optimise the measurement approach, the Poseidon-4 altimeter uses a 9 kHz PRF and an open-burst interleaved chronogram. It arranges the pulse transmit and receive chronogram in a manner that forces echo reception to occur in between (interleaved) transmitted pulses to increase the number of measurements over a given target. Measurements are then multi-looked at target locations on ground to reduce thermal and speckle noise by averaging at a resolution of ~300 m along-track. Interleaved mode timing doubles the number of available looks for SAR mode and importantly, allows SAR data acquisition simultaneously with true LRM data acquisition i.e. there is no instrument transition required between LRM and SAR mode. This is particularly important to characterise differences between the long-term historical LRM altimeter reference time series and new SAR measurements introduced by Sentinel-6. A pseudo-LRM mode (e.g. Dibarboure et al., 2014) has been used to study the differences between LRM and SAR (e.g. Moreau et al., 2018) using the CryoSat 2 and Sentinel-3 missions. Using pseudo-LRM measurements, it was possible to determine the pulse-to-pulse correlation effects (e.g. Walsh, 1982) on high PRF LRM altimeters, demonstrating some potential sea-state dependent discrepancies in the determination of SSH and Hs between previous Jason altimeters operating at 2 kHz PRF and the Poseidon-4 operating at 9 kHz PRF, (Egido and Smith, 2019). These discrepancies will need to be analysed and corrected in order for the Sentinel-6 measurements to be fully consistent with the geodetic data record.

4.2. Poseidon-4 measurement modes

The Poseidon-4 altimeter includes nine separate measurement modes using two chronograms: an acquisition chronogram and an interleaved chronogram. Apart from tracking acquisition, the interleaved chronogram is used which operates in an open burst configuration with a PRF of 9 kHz. Following the common approach of other altimeter designs (e.g. Steunou et al., 2015), the Poseidon-4 PRF is adjusted along the orbit using the vertical velocity of the satellite platform derived from the DORIS instrument. This is implemented for each tracking cycle in steps having a worst case ~2.5 m altitude variation per tracking cycle (~50 ms).

In order to address long-term stability requirements, Poseidon-4 implements a new calibration strategy. A heritage CAL-1 approach (e. g. as for Sentinel-3, Quartly et al., 2020) provides the instrument Impulse Response for both SAR and LRM by ignoring the antenna and looping back the transmit chain with the receive chain. This information is used to compensate for distortions in signal amplitude and phase

---

[1] The theoretical range resolution of Poseidon-4 with a bandwidth of 320 MHz is ~0.47 m. However, the altimeter clock is 395 MHz and a conversion of 0.47 m × 320/395 is required that results in a range sample of 38 cm. Thus, Poseidon-4 is a partially over sampled system.
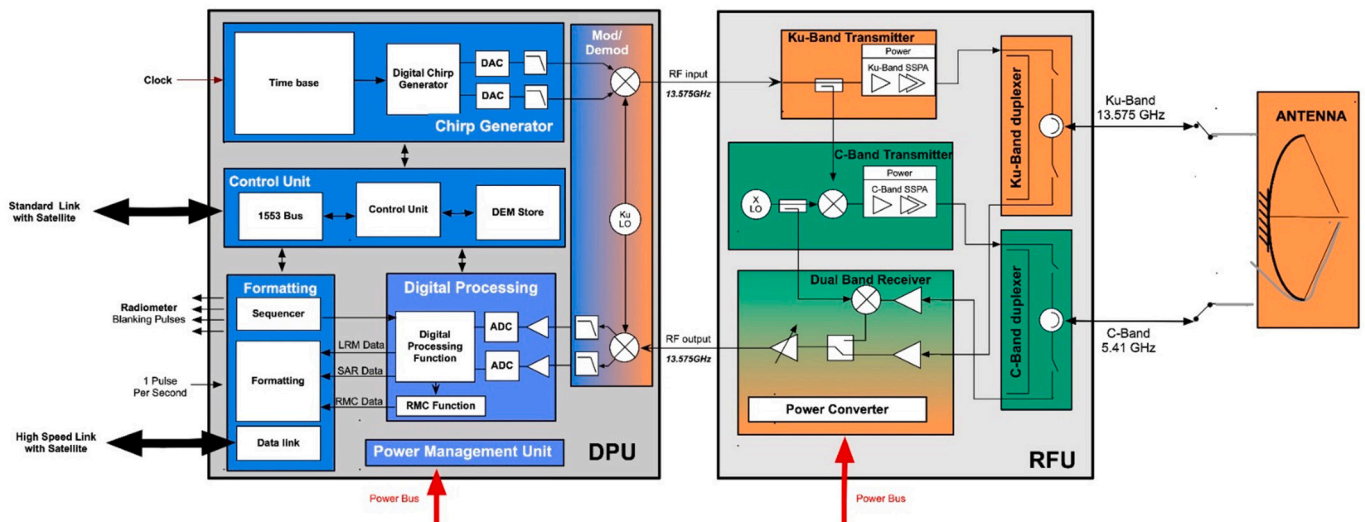
Fig. 4. Block diagram of the Sentinel-6 radar altimeter. Blue colours indicate digital electronics and orange colours analogue electronics. Green colours indicate a hybrid of the two. The Poseidon-4 instrument includes three main units. 1: The Digital Processing unit (DPU) that consists of the chirp generator and sequencer that generates digital chirps at the carrier frequency and at the instrument PRF. This is sent to the Radio Frequency Unit (RFU) via the Modulator/demodulator function. The DPU also contains the sequencing and control unit that holds the OLTC DEM and the digital receiver processing unit: this contains the core functions to process the received echoes from the RF unit. The processing unit includes a matched filter to de-compress the received chirps, selection of waveforms, the SAR high resolution (HR) data, waveform accumulation for the Low Resolution (LR) data (also used for closed loop tracking), and a Range Migration Correction (RMC) function and output. The formatting unit converts the processed LR, HR and RMC waveforms into formatted Instrument Source Packets (ISPs). 2: The RFU converts the Ku-band digital chirps into analogue Ku- and C-band pulses that are amplified for transmission through the duplexers to the antenna. Receive echoes are passed through the receive duplexer paths into a dual band receiver that tunes the power levels and up-converts the C-band pulses to Ku-band before sending the echoes to the DPU. 3. The antenna is the interface for transmission of Ku- and C-band pulses and reception of their echoes. The instrument digital and RF units are duplicated in a second instrument to increase redundancy, though there is only the one antenna. (For interpretation of the references to colour in this figure legend, the reader is referred to the web version of this article.)
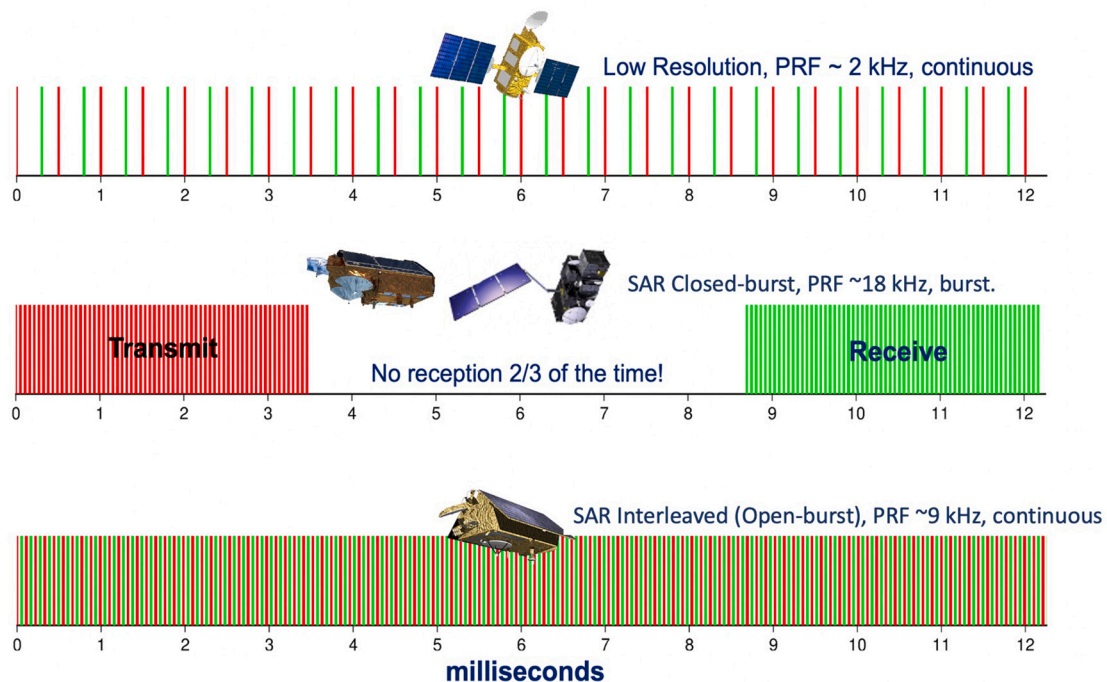

Fig. 5. Evolution of satellite radar altimeter chronograms highlighting the optimal use of available transmit and receive time when using the Sentinel-6 interleaved (open burst) measurement approach compared to Sentinel-3 (closed burst mode) and Jason series that provides LRM measurements only.

along the entire emission and reception bandwidth. The frequency of CAL-1 acquisitions will be determined from the measurements themselves during commissioning activities. A dedicated calibration pulse (termed CAL_ECHO) within each tracking cycle is also used to

continuously monitor instrument delay and amplitude variations along the orbit. Since amplification gain control knowledge directly impacts the σ^0 measurements, an attenuation calibration (CAL_ATT) is included in the design. This measures the top of the range impulse response

within the full attenuation dynamic range that is then matched to a corresponding value on ground. The CAL_ATT is then used during ground processing to correct the echo power used to estimate σ⁰. A Pulse Repetition Interval (PRI) calibration is implemented to characterise the internal Impulse Response (I&Q) of the instrument at each PRI step in flight. Although not required due to the digital architecture of Poseidon-4, a heritage CAL-2 is available to measure the transfer function of the receive and test the reception chain of the altimeter. The in-flight CAL-2 of S6-MF shows a slope of 0.02 dB over the window with no edge effects (there was ~0.1 dB of anti-alias filter effect seen on S3/CryoSat/Jason missions). Thus, in LRM, S6-MF uses the full analysis window of 256 × 0.38 m samples.

Both Open Loop (OL) and Closed Loop (CL) tracking are offered by Poseidon-4. OL tracking is particularly useful over coastal transitions and acquisitions over river and lake targets that present challenges to the CL tracking approach. The instrument uses a matched filter on receive with an on board range window of ~20,000 samples that is down sampled to 256 samples. Poseidon-4 uses a dedicated CL 2 kHz chronogram for initial echo 'acquisition mode' with a large 720 m window over a shorter radar cycle duration. DORIS instrument navigation data are also used to reduce time taken to establish altimeter tracking and minimise data loss when the instrument is switched between modes. Once an initial search, set and lock process is complete, the position of the tracking window is automatically adjusted on board to ensure continuous tracking using the 9 kHz interleaved chronogram. Following Sentinel-3 SRAL, the Poseidon-4 OL approach sets the position of the tracking window directly from pre-computed altitude values stored on-board the instrument in a one-dimensional Digital Elevation Model (DEM) called the Open Loop Tracking Command (OLTC, e.g. Le Gac et al., 2019). Position, velocity and time (PVT) coordinates derived from DORIS are used to look up the relevant OLTC values. The interleaved chronogram allows different configurations for the data on-board processing and data downlink summarised in Table 4.

Building on lessons learned from Jason-2, Jason-3, Sentinel-3A/B for coastal and inland water surface acquisitions, the OLTC has a much larger memory allocation of ~9 Mb compared to 1 Mb on the Jason-3 and 4 Mb on Sentinel-3A and B missions, respectively. This larger size means that more complex river and lake targets (where the terrain is often characterised by large elevation change river valleys) can be included. Sentinel-6 Poseidon-4 will be the first altimeter mission to use an uncompressed OLTC coded as 2 bytes (signed values). Contrary to the Jason-3 and Sentinel-3 missions, the OLTC is indexed by orbit (127 orbits for the Sentinel-6 reference orbit), in which each point is described by its angular position at a resolution of 0.01° for 36,000 positions within each orbit referenced and a vertical resolution of 1 m to the Earth Geoid. In this configuration, it is possible to upload in-flight a completely new DEM to the instrument or to patch any part of the DEM during closed-loop operation. Fig. 6 shows the current set of OLTC river and lake targets in the OLTC for S6-MF just before launch.

During commissioning, full resolution (LX2) data acquisitions will be used to gain experience of using and understanding the differences between LRM, raw SAR, and LRMC data on derived geophysical products over all surfaces. After a thorough analysis of these data and comparison to Jason-3 data, a final choice of operating mode will be made for the Sentinel-6 mission (e.g. LRMC over all surfaces potentially allow a larger acquisition of inland water retrievals using SAR data).

4.3. On-board range migration correction (RMC) processing

The purpose of the on-board Range Migration Correction (RMC) algorithm is to reduce data volume due to system constraints. The function aligns each burst of waveforms in range and selects a configurable number of samples for downlink to ground. The RMC function (Phalippou et al., 2012; Phalippou and Deemster, 2013) performs a truncation of the altimeter echo waveform and reduces the data rate by a factor of two. All RMC truncated data are transmitted for on-ground processing. An overview of the process is provided in Fig. 7.

A Fast Fourier Transform (FFT) is performed on each pulse of the burst to transform the input pulses from the time domain into the frequency domain and range data are then processed to centre the spectrum at the zero frequency. A fully configurable azimuth weighting mask with 64 values stored onboard is applied to compensate for power/phase distortions within a burst. A correction is then applied to each pulse in the burst to align the burst in range with respect to the extrapolated ellipsoid-normal (radial) velocity derived from the 0.1 Hz DORIS state vector. This allows a lossless reversal of the on-board RMC processing to be performed on ground. A Doppler centroid correction is employed to compensate for changes in orbit altitude rate that otherwise would cause errors depending on the ellipsoid-normal (radial) velocity. After buffering, 64 Doppler beams are formed for each burst in azimuth. An RMC matrix stored on-board the instrument is applied to each burst that aligns the pulses at the leading edge that is calculated for fixed mean values of altitude, satellite velocity and PRF. This is fully configurable in-flight, though expected not to change once tuned shortly after launch. Following an inverse FFT to convert to the time domain the final step is to truncate the waveform by removing all samples after 128 range bins. Fig. 8 shows the resulting waveform and impact of removing 128 range bins from the waveform trailing edge in terms of waveform power. While the RMC on-board processing is reversible on ground, the removed part of the waveforms cannot be recovered.

The retrieval of ocean parameters from satellite altimetry waveforms fits the returned echo to a theoretical model (e.g. Halimi et al., 2014). A different model is used for LRM and SAR (e.g. Ray et al., 2015; Recchia et al., 2017) since a SAR altimeter waveform has a distinctly different shape compared to an LRM waveform (see Fig. 9). While most of the information is contained in the first half of the SAR waveform, significant effort has been dedicated to simulating the impact of truncated SAR waveforms on the performance of Sentinel-6.

The performance of on-board processing depends on the ability of the RMC matrix to represent in-flight conditions. The ellipsoid-normal

Table 4
Summary of available Sentinel-6 Poseidon-4 configurations.

| ID (closed Loop = CL, Open Loop = OL)	Description
LRM_CL	Conventional LRM echoes acquired with a low PRF and provided as power samples over the range window
LX_CL	Raw SAR I and Q echoes in the frequency domain (i.e. without any on-board Range Migration Correction (RMC) processing together with LRM measurements
LRMC_CL	LRM together with SAR measurements after on-board RMC processing (reversible on ground) has been applied to reduce data volume.
LX2_CL	LRM measurements, raw SAR I and Q data and SAR RMC data. The LX2_CL mode is the only mode that allows Poseidon4 to download the LRM, SAR and RMC data for the same time and location. It is designed to validate the on-board RMC processing by reversing, on-ground, the RMC applied by the on-board processor. This mode cannot be used as routine mode due to the considerable amount of data that is generated
LRM_OL	LRM data only (heritage mode for reference altimeter missions and useful during early commissioning activities).
LX_OL	LRM and SAR I&Q data
LRMC_OL	LRM and SAR I&Q data after on-board RMC processing is applied
TPX	Transponder mode: this is a specific mode for external calibration over targets sites with well-known location and characteristics. OL tracking is used with a fixed instrument gain and initial satellite-terrain height tracking instruction to provide LRM, SAR RMC and SAR I&Q data. Transponders, if used, should not exceed a maximum power level of 6.7 dBm in Ku-band and − 6.75 dBm in C-band in order not to damage the Poseidon4 receiver or degrade the measurements.
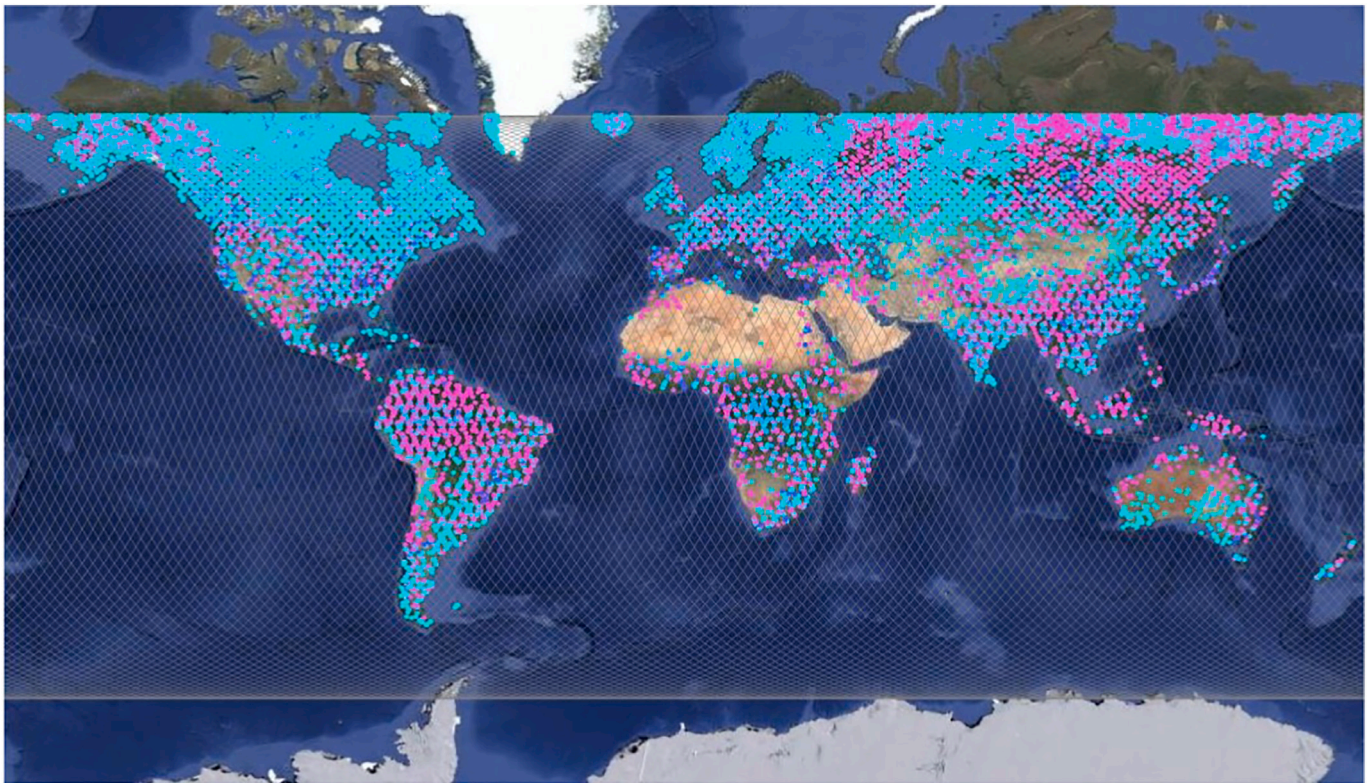
Fig. 6. Locations of river and lake targets within the Sentinel-6 Poseidon-4 OLTC. The OLTC currently accommodates 31,805 targets of which 8655 define rivers, 21,666 define lakes, 1484 define reservoirs with no targets defined yet for glaciers. (see https://www.altimetry-hydro.eu/ for more information Credit: D. Blumstein, CNES/LEGOS and S. LeGac, CNES).
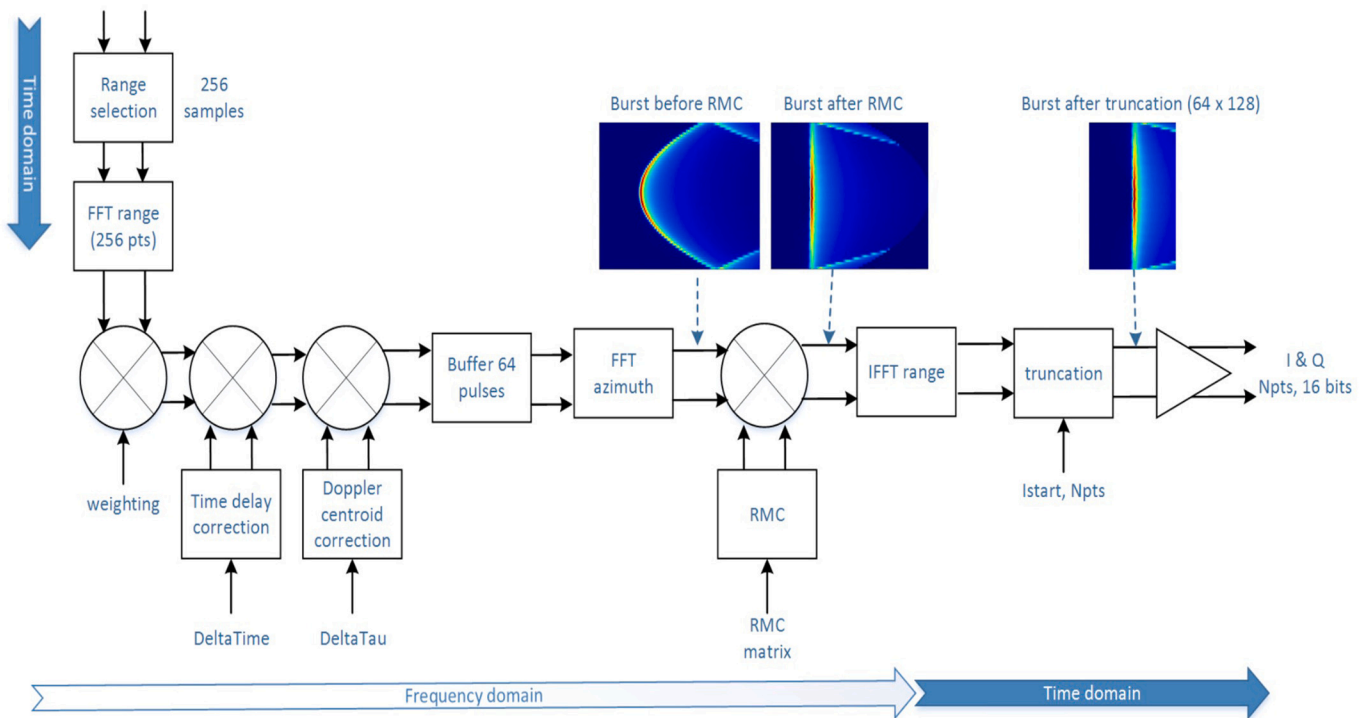

Fig. 7. Simplified block diagram describing the Sentinel-6 on-board Range Migration Correction (RMC) processing. The example images are for illustration purposes only.
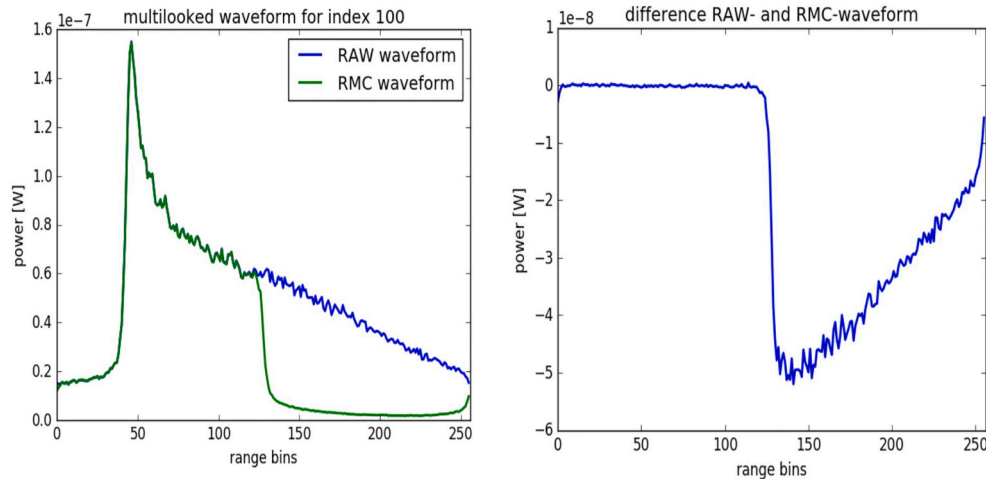
Fig. 8. Comparison of SAR waveform and corresponding reconstructed waveform after the RMC process has been reversed highlighting the negligible differences in the first part of the signal after truncation.
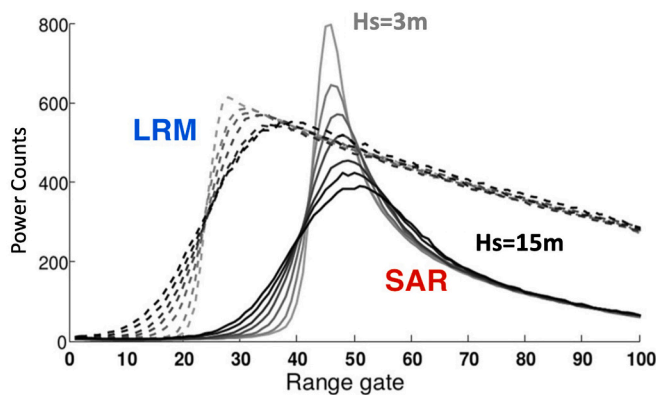

Fig. 9. Different characteristic waveform shapes for SAR and LRM echoes at different Hs highlighting the peaked form of a SAR return. The figure shows averaged SAR (solid) and pseudo-LRM (dashed) waveform from Sentinel-3 for Hs = 3,5,7,9,11,13 and 15 m, for cycle 23 orbit 349, on 25 October 2017 in the Pacific (after Ardhuin et al., 2019, modified by G. Quartly with permission).

(radial) velocity is extrapolated from the on-board DORIS navigation information provided with an uncertainty of 1.5 mm s^{-1} every 10 s. The actual velocity for each pulse depends on the extrapolation algorithm but is expected to be at the same order of magnitude. However, in certain parts of the ocean there can be significant slopes in the geoid (Fig. 10) which cause the ocean-surface-normal velocity to depart from the ellipsoid-normal velocity. While the OLTC ~1 km horizontal and 1 m vertical resolution captures most variation (based on the mean sea surface derived from altimeter measurements and models) some differences may remain. These may be sufficient to misalign the central beam of the burst within the azimuth window and of the stack of waveforms being processed. In this condition, the RMC processing may not be able to align the leading edge properly and the Doppler bins are not aligned orthogonally to the range bins. Simulations show that a 100 μrad surface slope will lead to a misalignment of up to 3 range bins within the burst leading to a loss of 3 range bins after truncation. An extreme along-track slope of about 360 μrad, as simulated in Fig. 11, results in the loss of up to 11 range bins.

In order to compare the performance of the parameter retrieval algorithm between unprocessed SAR and RMC SAR data before launch, several simulations have been conducted and analysed. These focused on comparisons between unprocessed SAR and RMC processed data for the same simulation of derived SSH, Hs and the normalised backscatter

coefficient σ^0. The Sentinel-6 mission performance simulator (S6MPS) simulated instrument source packets (ISP) that were further processed using the Sentinel-6 Level 1b Ground Processor Prototype (GPP), to reverses the on-board RMC processing before applying the SAR processing chain. After masking the model for the truncated data, parameters were estimated with a Levenberg-Marquardt curve-fitting algorithm using the waveform model described in Recchia et al. (2017). The most extreme case considered Hs = 8 m, a surface slope of 360 μrad with an altitude change rate of 15.5 ms^{-1}. Results are shown in Fig. 12 and other more realistic simulations that show lower errors are reported in (ESA, 2018).

Based on these simulations, the on-board RMC processing is not expected to affect the performance of Sentinel-6 level 2 products. This holds for nominal situations with different altitude rates and for extreme cases of sea surface slope not taken into account by the on-board RMC processing. Preliminary in-flight performance of the RMC is reported in later sections confirms this finding.

5. Advanced microwave radiometer for climate (AMR—C)

To accurately monitor ocean parameters, Poseidon-4 altimeter measurements require an accurate determination of wet tropospheric PAth Delay (PD) over a range of 0–40 cm. The water vapour content within the troposphere exhibits large spatial and temporal variability which is difficult to model commensurate with the space and time resolution of the altimeter measurement (Brown, 2013). Instead, the Advanced Microwave Radiometer for Climate (AMR—C) is designed to provide data necessary to correct Poseidon-4 radar pulses for this effect. The contribution of the wet troposphere PD to the overall altimeter-derived SSH error budget is set at ≤1.2 cm for Near Real Time (NRT, 3 h from data acquisition) and Short Time Critical (STC, 36 h from data acquisition). For Non Time Critical (NTC, 60 days from acquisition) the requirement is ≤0.8 cm (all performance as RSS at 1 Hz for a typical sea of 2 m Hs and 11 dB σ^0 at 1 s along-track data rate). In addition to PD, the AMR-C also provides an atmospheric attenuation correction of the altimeter surface backscatter due to rain, clouds and water vapour (e.g. Ruf et al., 1995). In non-precipitating conditions it is ≤0.007 dB for C-band and ≤ 0.05 dB for the Ku-band radar frequency. In precipitating conditions, it is ≤0.05 dB and ≤ 0.5 dB for the C-band and Ku-band radar frequency, respectively.

The AMR-C instrument (Fig. 13) is an evolution of the AMR developed by NASA-JPL, for Jason-2 and Jason-3, which itself was based on the TOPEX Microwave Radiometer (TMR) and Jason Microwave Radiometer (JMR) embarked on the TOPEX/Poseidon and Jason-1 missions respectively (e.g. Brown et al., 2004; Maiwald et al., 2016). It measures
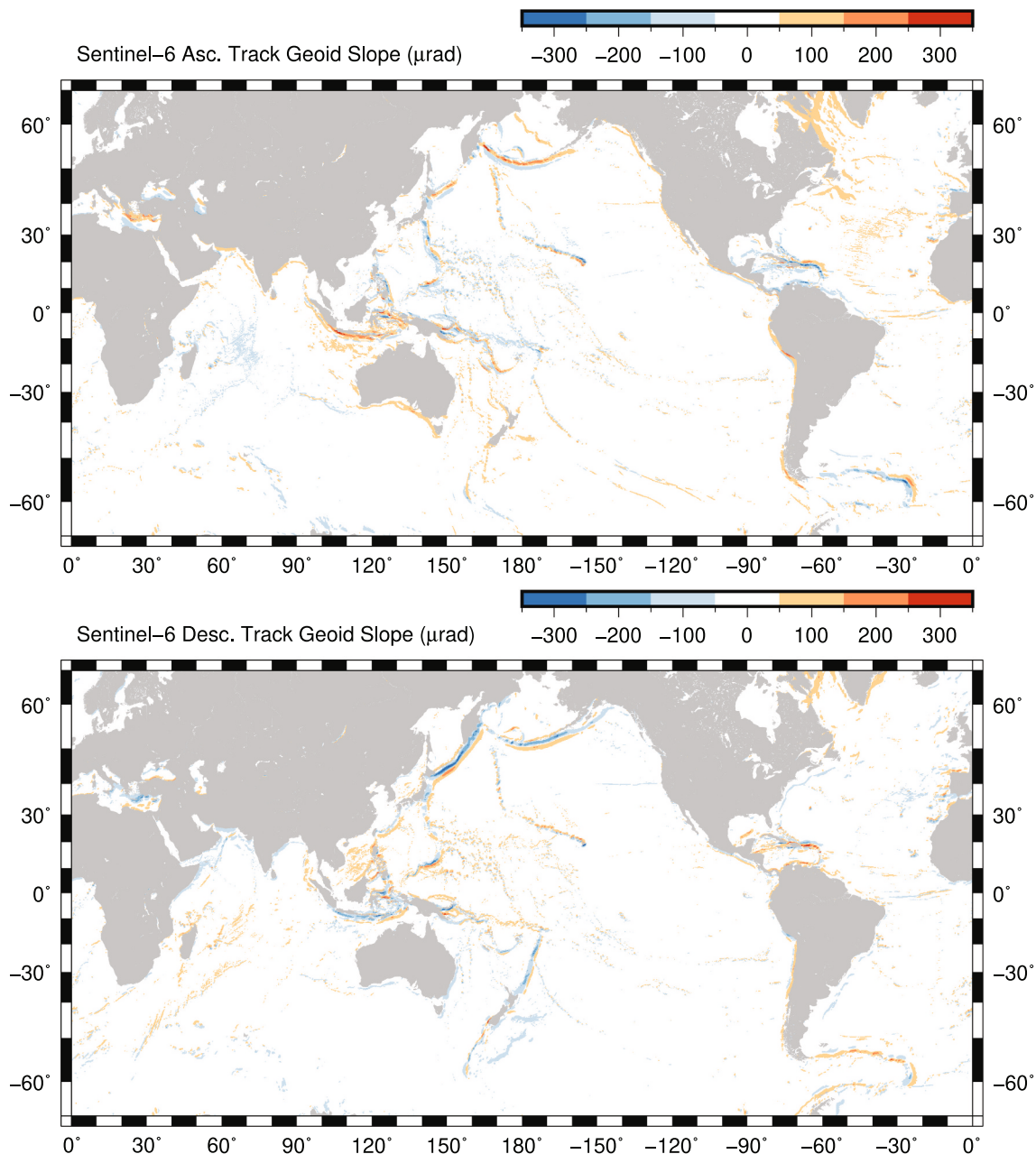
Fig. 10. Estimated global Sentinel-6 along-track slope in the ascending (top) and descending (bottom) directions, in micro-radians (1 μrad = 1 mm change in geoid height per 1 km of movement along the surface of the ellipsoid) computed using Jason-3 Cycle 55 as a proxy for the Sentinel-6 ground track and projecting the global north and east components of slope into the along-track slope component on the ground track.

linear polarized brightness temperature (TB) at 18.7, 23.8 and 34 GHz. It uses an internal reference load and three noise diodes for short-term calibration, which is performed autonomously as part of the nominal measurement cycle. The three-frequencies are used to separate the three dominant components of the TB signal to estimate wet PD: total atmospheric water vapour, total integrated cloud liquid water and wind induced ocean surface roughness (e.g. Fernandes et al., 2015). The instrument is dual linearly polarized, with one polarization being the nominal radiometer side and the other polarization being the redundant side. Since observations are acquired at nadir, polarization only has a weak dependency on surface roughness and its orientation (Tran et al., 2002; Francis, 2002). The nominal instrument polarization is oriented perpendicular to the ground track and the redundant instrument polarization is oriented parallel to the ground track. The spatial resolution of the measurements in all channels is less than 35 km and the antenna

beams are equalized in the along-track direction by averaging and therefore only differ slightly across-track (Brown, 2006).

For a measurement system designed to act as a reference and monitor sea level rise, it is critical that any drift in the AMR-C be accounted for since this has a direct impact on the quality of Poseidon-4 measurements and the ability of the measurement system to track variations of the global mean sea level. Experience with the microwave radiometers on TOPEX/Poseidon and Jason-1 has shown they are susceptible to small but systematic calibration issues (e.g. Brown, 2013, Brown et al., 2009). Sentinel-6 sets a long-term PD stability of ≤0.7 mm (standard error) averaged over any one year period for NTC products. To address this requirement, an external supplemental calibration system (SCS) has been developed which is used to maintain the long-term stability over mission life. The SCS includes a small reflector placed between the radiometer feed horn and the main reflector that directs the AMR-C
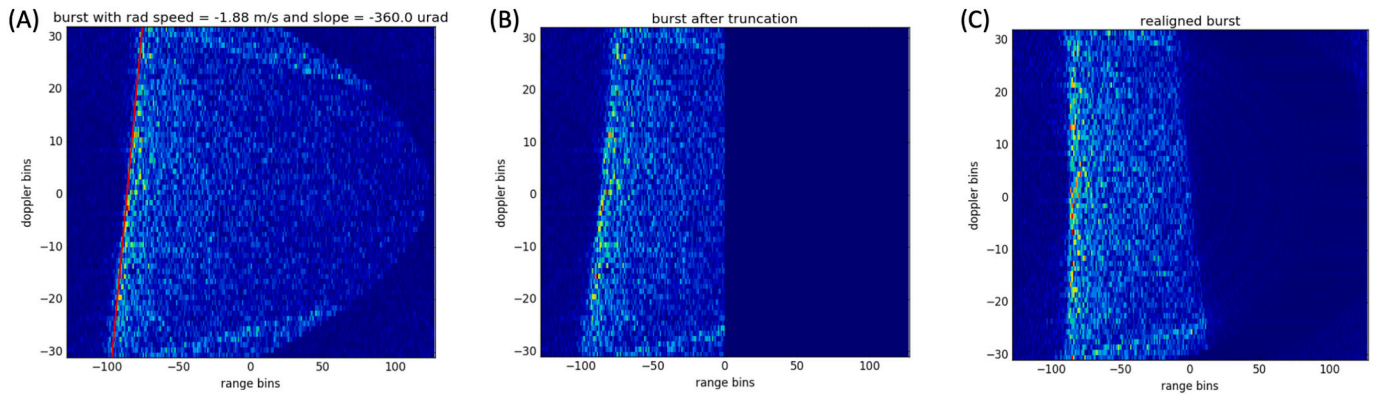
Fig. 11. (A) Simulated burst over a surface slope of −360 micro radians before RMC processing. (B) Burst after truncation and after realignment and (C) Realigned and truncated burst. The loss of ~11 range bins at the tail of the echoes can be observed.
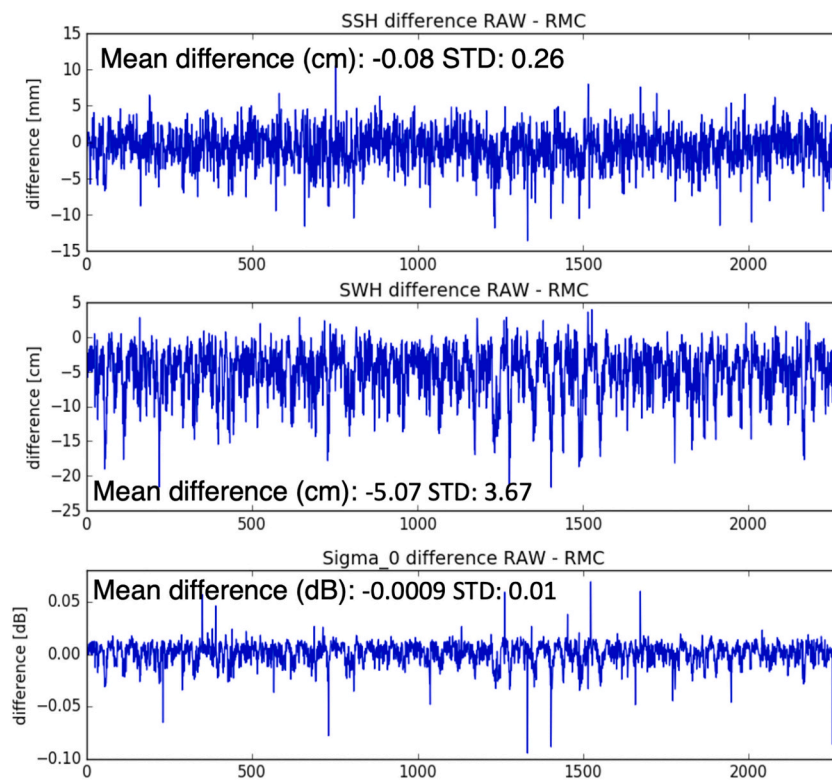

Fig. 12. Comparisons between simulated RAW and RMC mode for the same simulation of the following retracked parameters: SSH, Hs and the normalised back-scatter coefficient σ0. All simulations are based on output from the S6MPS and GPP.

beam to a blackbody warm calibration target maintained at ~300 K or to cold space (~3 K). During each SCS calibration (every five days when the satellite is over land), the cold space and warm target are used to calibrate the radiometer internal calibration sources; noise diodes (gain) and reference termination (offset). Using the SCS, the AMR-C can be accurately and swiftly calibrated without changing the orientation of the entire spacecraft to point at the cold sky or waiting for passage over a vicarious target on Earth (Maiwald et al., 2020). The AMR-C SCS is predicted to provide long term stability to 0.07 K yr^{-1} relative to 0.1 K yr^{-1} requirement based on 5-day SCS calibration cadence.

In addition to the SCS, a periodic cold sky calibration satellite pitch manoeuvre is used to point the AMR-C main antenna beam instrument feedhorns at a cold sky location. This provides a stable baseline deep space view 2.7 K signal to the instrument with a minimum Earth contribution in the antenna back lobes. This approach ensures a cold

calibration through the entire measurement path, including the main reflector. This information will be used to calibrate the cold sky mirror of the SCS. In this way, the long-term calibration of the SCS will be independently checked against on-ground vicarious reference targets as well as cold-sky every 10–30 days (to be refined based on in flight analysis).

In total, five radiometer systems were built, two for each AMR-C and one spare and prelaunch performance shows a measurement noise of 0.13 K (Maiwald et al., 2020). After antenna temperature calibration and pattern correction an RSS uncertainty in brightness temperature at 1 Hz of 0.25 K, a 0.3 K system margin is achieved. Using a representative radiative transfer model to simulate TBs and compute PDs from numerical weather model geophysical fields (Brown et al., 2004), PD error has been mapped to brightness temperature error using the PD retrieval algorithm, which provides a sensitivity for each channel following
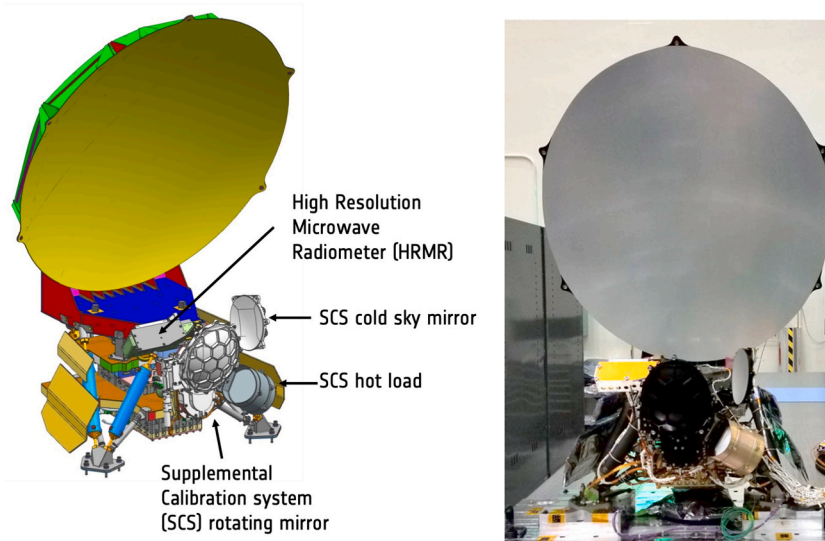
Fig. 13. The Advanced Microwave Imager for Climate (AMR—C). See Maiwald et al. (2020) for a full description of the Sentinel-6 AMR—C.

Keihm et al. (1995). The pre-launch performance estimates by this analysis indicate a 1 Hz measurement AMR-C PD uncertainty of 0.62 cm.

5.1. High resolution microwave radiometer (HRMR)

The troposphere affects the altimeter radar signal at various time-space scales, from high frequency - in the vicinity of fast moving atmospheric fronts and near the coasts - to low frequency and large scales over open ocean. The relatively large ground footprint of the AMR-C 18–34 GHz channels remain the baseline inputs for Sentinel-6 to determine WP delay over the open ocean but near coastlines, the retrieval error significantly increases due to antenna beam contamination by warm landmasses (e.g. (Desportes et al., 2007, Lázaro et al., 2019). For Jason-2/OSTM, the impact of land contamination in the measurement field of view increases rapidly ~30 km from the coastline with a minimum residual variance at 40 km (Sibthorpe et al., 2011).

To support the high resolution SAR mode from the Poseidon-4 SAR altimeter in the coastal zone, an experimental high-resolution

microwave radiometer (HRMR) AMR-C subsystem was developed (Kangaslahti et al., 2019) to provide high spatial resolution measurements at 5 km resolution. HRMR includes millimetre-wave channels at 90, 130 and 168 GHz with good sensitivity in the atmospheric water vapour continuum. The HRMR has a sensitivity (Noise Equivalent Difference Temperature, NEΔT) of better than 0.2 K and stability of 0.2 K for all three frequencies over 60 s. HRMR shares the primary reflector with AMR—C. Since off-axis operation at higher frequencies results in beam distortion, the HRMR must be on the primary optical axis. Data from these channels will extend the WP delay retrievals closer to the coast under cloud-free conditions on an experimental basis. In operation, HRMR data will not use the calibration targets of the AMR-C SCS but will be cross calibrated based on the AMR measurements over ocean targets before coastal transitions occur. See (Maiwald et al., 2020) for a full description of the Sentinel-6 HRMR.

Fig. 14 (left) shows the HRMR and AMR-C beam placements in the coastal zone, and (right) simulated combined AMR-C and HRMR retrievals in the coastal region: the benefit of the HRMR smaller footprints
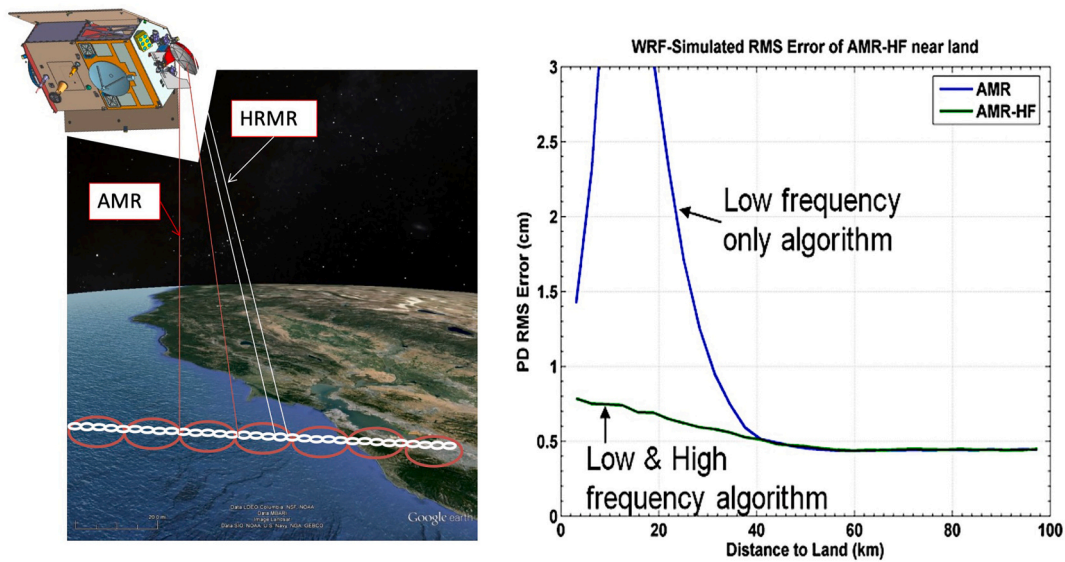

Fig. 14. (left)A)) approximate beam placements for the AMR-C low frequency channels and the HRMR high frequency channels when approaching the coast. (right (B)) simulated error for PD retrievals when using AMR-C low frequency channels and combined processing of AMR-C and high frequency HRMR channels in the coastal zone.

together with AMR-C footprints after coastal processing techniques have been applied is clearly evident within 40 km of the coastline.

The AMR-C PD retrievals will be validated using comparisons with ground-based radiometers, and radiosonde soundings, as well as other space-based radiometers (for example, SSM/I). The AMR-C performance and calibration on-orbit will be monitored using heritage approaches developed over past decades of altimetry with additional efforts specific to characterise SCS including vicarious ocean targets, Amazon forest areas (providing a 'hot' reference) and inter-satellite comparison within the altimetry constellation. In addition, comparison to numerical weather model derived PD and wind speeds will be used.

6. Radio occultation (GNSS-RO)

Sentinel-6 includes a GNSS Radio Occultation (GNSS-RO) payload as a secondary mission element to determine atmospheric temperature and humidity profiles by measuring bending angles of GNSS signals occulted by the Earth's atmosphere (e.g. Kursinski et al., 1997). GNSS-RO measurements provide atmospheric vertical temperature profiles with good vertical resolution (~0.5–2 km) in the upper-troposphere to the middle stratosphere (~8–35 km). Data from the Constellation Observing System for Meteorology, Ionosphere and Climate/Formosa Satellite Mission 3 (COSMIC/FORMOSAT-3, Anthes et al., 2008) show a positive impact on Numerical Weather Prediction (e.g. Healy et al., 2020) and consistency of global temperature reanalyses in the lower and middle stratosphere (e.g. Long et al., 2017; Ho et al., 2019). Other applications include spatial maps of balanced GNSS-RO monthly mean zonal and meridional winds (Scherllin-Pirscher et al., 2014, Verkhoglyadova et al., 2014, Healy et al., 2020). The Sentinel-6 GNSS-RO is designed to retrieve ~1000 occultations per day, provide L1b and L2 products within 3 h (90%) using measurement ray path tangents from ~8 km extending up to ~500 km altitude.

The Sentinel-6 GNSS-RO receiver was developed by NASAJPL based on the TriG sensor (e.g. Ho et al., 2019). The Sentinel-6 high elevation, low inclination non sun-synchronous drifting orbit was studied to determine the requirements and performance of GNSS-RO. In conclusion, two GNSS-RO antennas are deployed on Sentinel-6: one on the forward (Fig. 15) and a second on the aft external bulkheads of the
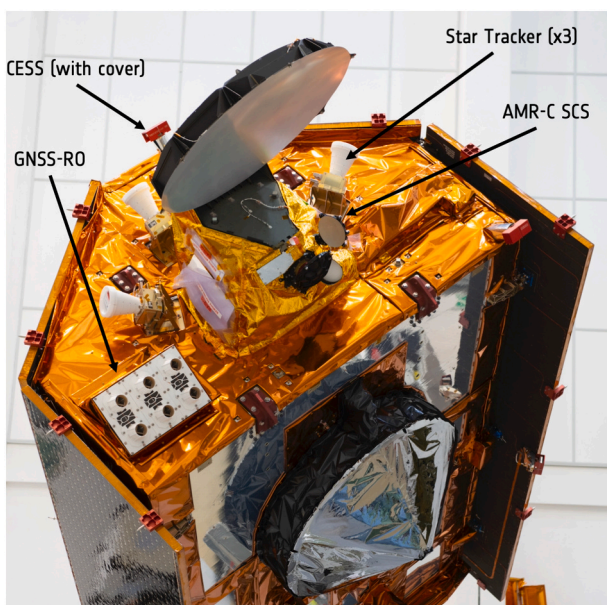

Fig. 15. Photograph of the NASA GNSS-RO receiver antenna subsystem embarked on Sentinel-6 together with star tracker and the AMR–C. The Poseidon-4 antenna is visible and covered by a protective blanket ready for flight.

satellite. A dedicated GNSS antenna for the GNSS-RO is located on the satellite roof.

7. Radiation environment monitor (REM)

The high altitude inclined orbit of Sentinel-6 is closer to the proton belt than typical Low-Earth Orbits satellites, which induces a much harsher radiation environment for the on-board electronics. Like the CARMEN-2 on-board Jason-2 and -3, Sentinel-6 hosts a Radiation Environment Monitor (REM) in order to correlate any on-board event with radiation effects and to measure the space radiation environment. The REM instrument counts high-energy particles using extremely sensitive detectors and follows the long heritage of the Standard Radiation Environment Monitor flown on many ESA satellites (Desorgher et al., 2013). Processed measurements will be ingested in the ESA Space Weather processing chain.

8. Precise orbit determination (POD) complement

Accurate determination of the satellite orbit is a fundamental component of the Sentinel-6 mission that is primarily dedicated to estimates of sea level. Table 1 shows that NRT orbit determination of 5 cm or better (goal is 3.0 cm) is required in the radial component after all processing. The NTC requirement is 1.5 cm (with a goal requirement of 1 cm). The Sentinel-6 GNSS-POD multi-frequency receiver is designed to measure the position of the satellite and operates using existing GPS satellites and European Galileo satellite systems (e.g., Johnston et al., 2017; Hein and Pany, 2002). In addition to a larger number of satellites for position fixing, Galileo signals are expected to bring greater performance. Two GNSS-POD units are included in a redundant configuration that can track up to 24 single frequency channels with a single frequency tracking scheme or up to 18 GNSS satellites using a dual-frequency tracking scheme. Each is designed to deliver real-time orbit position and orbit velocity measurements in the WGS 84 Earth centred fixed frame coordinates, and time measurements with respect to UTC and GPS system time. The GNSS-POD unit provides the internal pulse-per-second timing information to all the equipment on board the satellite including the payload.

A large number of GNSS signals can be exploited by the Sentinel-6 GNSS unit including L1, L2, L5 and Galileo E1 and E5. Ionospheric attenuation of signals is corrected using a differential technique based on two signals at different frequencies. The 3D velocity of the spacecraft (at 3σ accuracy) must be better than 0.12 m s^{-1} at 1 Hz sampling rate (when selective availability is not enabled) with pre-launch analysis indicating an expected performance of 0.0042 m s^{-1} (99.7%). The real-time on-board horizontal positioning accuracy (circular error) must be better than 4 m with pre-launch analysis indicating an expected performance of 1.01 m (95%). This is required to control the altimeter open-loop tracking operations and platform navigation. Further ground processing computes satellite altitude with improved accuracy to meet the requirements for Sentinel-6 within the Copernicus POD Service (e.g. Fernandez et al., 2015). The GNSS-RO will also provide supplementary data for POD by means of positioning provided via the dedicated GNSS-RO POD antenna also accommodated on the roof of the satellite.

A DORIS sub-system (e.g. Nouël et al., 1988; Jayles et al., 2006; Auriol and Tourain, 2010) provides geodetic navigation packets including the satellite altitude variation rate with respect to the reference ellipsoid surface to an accuracy of 0.1 mm s^{-1} at a resolution of 0.1 mm s^{-1} sampled every 10 s. The instrument includes a new design ultra-stable oscillator (RK410 mini-USO) that provides the clock for the Poseidon-4 precise retrievals and positional information allowing improved altimeter surface tracking. The DORIS 1 Hz reference atomic time pulse has a design accuracy of 5 microseconds or better at a resolution of 100 ns providing a datation accuracy of 1–2 microseconds (e.g. Jayles et al., 2016). These measurements are used to derive the on board real time orbit determination (DIODE; Jayles et al., 2002) with position,

along-track and cross-track components <1 m RMS (ITRF or Geodetic reference frame), with ellipsoid-normal (radial) component position less than 5 cm RMS (ITRF) and the velocity of each component <0.001 m s^{-1}, at 1-σ (ITRF or Geodetic reference frame). The DORIS altitude variation rate is also used to centre the Doppler frequency map in the RMC compression of the altimeter.

A Laser Retroflector Array (LRA) developed by NASA is included in the mission to support independent ground-based laser tracking for precise orbit determination and validation. Laser tracking provides ranging to an accuracy of <2 cm and will be used throughout the Sentinel-6 commissioning phase and operationally during the mission for SLR-based POD validation. The LRA is a small passive optical device consisting of quartz corner-cubes that directly reflect an incident laser beam compatible with Satellite Laser Ranging stations operating at wavelengths of 532 nm and/or 694 nm (Pearlman et al., 2002).

9. Ground segment and mission products

The Sentinel-6 mission product definitions are mainly derived from the Sentinel-3 and Jason-3 products definitions and a full overview of products can be found in Scharroo et al. (2016). These are summarised in Table 5.

The primary altimetry mission provides three operational data services with different levels of products, delivery timeliness tuned to applications with different mission performance (see Table 5). NRT Altimetry Service (ALT-NRT) Level 2 products are available to end-users within 3 h of acquisition. They include Hs and wind speed, primarily for meteorological services. SSH has a has lower accuracy compared to STC and NTC products dues to the use of preliminary orbit information and predicted meteorological corrections. STC Altimetry Service (ALT-STC) Both Level 1 and Level 2 products are available to the end-users within 36 h after data acquisition. They include Hs and Wind Speed and a more accurate SSH using improved ancillary data (e.g., orbit altitude, meteorological models, etc). These data are designed for ocean modelling and assimilation by ocean models. ALT-STC Level 1A products will provide high-resolution individual echoes, while the Level 1B products contain the high- and low-resolution waveforms, both with additional instrument and calibration information for use by teams using alternative altimeter retracking techniques with a short latency. NTC Altimetry Service (ALT-NTC) Level 2 products are available to end-users within 60 days after data acquisition. The ALT-NTC Level 2 products are derived

Table 5
Sentinel-6 data products and delivery timeliness (HR = High Resolution, LR = Low Resolution). See Scharroo et al. (2016) for a complete review.

Near-Real Time: Level 2P HR, Level 2P and Level 3 LR Wind/Wave	Short Time Critical: Level 2P and Level 3 HR	Non Time Critical: Level 2P and Level 3 LR and HR
Mainly for operational Met agencies (wind and wave) Products split by satellite dump/granules (per ground station/10-minute chunks) NetCDF and BUFR	For ocean modelling and assimilation Product split by pass (pole to pole) NetCDF	Highest quality intended climate studies and research Products split by pass (pole to pole) NetCDF
3-h latency	36-h latency	60-day latency
Level 2: Low- and high-resolution products Standard (1-Hz and 20-Hz) Reduced (1-Hz) BUFR (1-Hz and 20-Hz) Level 2P: Harmonised L2 (1-Hz) MWR Level 2: 16-Hz AMR measurements	Level 1A: Individual echoes (HR only) Level 1B: LR and HR Level 2: LR and HR Standard (1-Hz and 20-Hz) Reduced (1-Hz only) Level 2P: Harmonised L2 (1-Hz) Level 3: With orbit error correction, error information (1-Hz) MWR Level 2: 16-Hz AMR measurements	Level 1A: Individual echoes (HR only) Level 1B: LR and HR Level 2: LR and HR Standard (1-Hz and 20-Hz) Reduced (1-Hz only) Level 2P: Harmonised L2 (1-Hz) Level 3: With orbit error correction, error information (1-Hz) MWR Level 2: 16-Hz AMR measurements

using precise ancillary data (e.g., final orbit altitude and meteorological models) and calibrations to provide the highest quality data products for operational users. Level 2P products are mono-mission along-track products with enhanced geophysical corrections and bias correction derived with other missions. They have the same sampling intervals as Level 2 products. For continuity with the Jason-3 mission, Level 2P SSH products will be provided as low-resolution products in NTC latency. Other Level 2P products include: high-resolution SSH (all latencies), high-resolution wind speed and Hs (NRT latency only). Level 3 products are global mono-mission along-track products with adjustment of orbit errors, editing, error information, as well as regional mono-mission along-track products derived from the corresponding Level 2P products. Both 1-Hz and 5-Hz sampling rates are planned.

The Sentinel-6 product suite includes an AMR Level 2 product containing measurements from the AMR-C instrument at the native sampling rate of approximately 16 Hz. These new products serve users that want to exploit the water vapour information for atmospheric modelling and are produced at all latencies (NRT, STC, and NTC). Only NTC products apply the final calibrations computed using data from the AMR-C SCS measurements.

As part of the product baseline, every 1 to 2 years a reprocessing of all NTC products is planned. In this way, all historical data will be upgraded using the most recent knowledge of instrument behaviour, improved ancillary data, enhanced algorithms, etc., as implemented in the product processors. This approach is fundamental to achieving and maintaining the goals of Sentinel-6 as a reference altimeter mission.

10. Early results from Sentinel-6 Michel Freilich

On 21st November 2020 S6-MF Launch and Early Operations (LEOP) began. The satellite was launched on a SpaceX Falcon 9 vehicle from the Vandenberg Air Force Base in California, US, at 17:17 UTC. The satellite was injected into orbit 18 km below Jason-3 prior to tandem flight acquisition manoeuvres. During this period, the LEOP was completed by ESA teams and the mission flight control was handed over to EUMETSAT on 24th November 2020. On November 30th, the Poseidon-4 altimeter instrument was switched on.

The DORIS unit Ultra Stable Oscillator (the RK410 mini-USO is a new model for this equipment) is performing extremely well with a stability performance of 5.10^{-14} s over a 100 s period and $0.007.10^{-8}$ s over 1.5 days (factor ~ 10 improvement from previous models). The DORIS datation accuracy is better than the 2 μs specification.

The first Sentinel-6 GNSS data (that includes Galileo and GPS) were available on 26–27 November 2020 and the initial analysis by ESOC's Navigation Support Office immediately showed a very good GNSS data quality. The performance from the GNSS POD shows that all instruments are functioning within expectation. This is the first Earth satellite that makes use of both the Galileo and GPS constellations. Initial analysis show that Galileo brings enhanced quality and performance compared to GPS receivers flown on previous Copernicus missions. This means that the orbit determination of Sentinel-6 will likely be one of the best available today - significantly reducing the uncertainty in sea level rise estimates. Future development of the Galileo High Accuracy Service (HAS) is likely to bring further improvement for future missions.

Initial measurements obtained from short passes over ocean with nominal satellite pointing show an overall estimated mis-pointing of ~0.01deg^2 derived from LRM MLE-4 re-tracking measurements and ~ 0.01° pitch based on SAR analysis. The Poseidon-4 interleaved impulse response calibrations (termed ECHO_CAL) that are recorded every 0.1 s shows a noise level of between 0.2 and 0.3 ps. The transfer function amplitude reveals a very small slope of ~0.02° over the full signal with random noise standard deviation of 0.01°. This compares with a variation of around 0.1° for CryoSat-2 SIRAL and Sentinel-3 SRAL from which a random noise level extraction is not possible since they are dominated by features of the respective radar design (anti-alias and digital filters).

Scientific justification and relevat requirements have been

Table 6

Preliminary range and Hs noise estimates (standard deviation) over the ocean surface of S6-MF Poseidon-4 compared to Sentinel-3A SAR and Jason-3 LRM data during the in the first 2-weeks of tandem flights. Measurements are for Hs = 2 m, σ^0 = 11 dB at 1 Hz for STC processed data.

	S3A SAR	S6MF SAR	Jason-3 LRM	S6-MF LRM
Radar Range STD (cm)	5.0	3.2	7.0	6.2
Hs STD (cm)	38.0	22.0	50.0	41.0

established (Donlon et al., 2019) for the Sentinel-6MF mission to perform a 12-month tandem flight in which it will follow the Jason-3 satellite 30 s in time on the same ground track. Following system checks, a series of manoeuvres were initiated to bring the satellite into a Tandem flight configuration with Jason-3 that was achieved on 18th December 2020 with S6-MF flying 30 s behind Jason-3. A tandem flight is particularly important since Sentinel-6 introduces SAR altimetry into the reference altimeter orbit time series for the first time, to reduce uncertainties in the measurements (e.g. Moreau et al., 2018; Reale et al., 2020; Ablain et al., 2009; Zawadzki and Ablain, 2016). Furthermore,

differences associated with long-wave swell signatures aliasing into the SAR radar footprint compared to heritage LRM measurements, have potential to introduce temporal and seasonal biases and impact the stability of the altimeter time series (e.g. Ablain et al., 2019). A tandem calibration phase is also essential to computing accurate sea level relative biases between two altimeter missions and link their global and regional MSL time series (Leuliette et al., 2004; Dorandeu et al., 2003) to GCOS requirements (Zawadzki and Ablain, 2016). Furthermore, the only viable way to effectively cross-calibrate the backscatter (wind speed) and wave height measurements in a short time period is via tandem flights (e.g., Quartly, 2009).

Limited processing of Posiedon-4 SAR and SAR-RMC data has been performed using preliminary data available from the first few days of operations. Initial results demonstrate exceptional performance in terms of the fundamental calibration parameters and science data in all radar modes. Table 6 shows preliminary noise performance estimates of the Poseidon-4 altimeter radar range and Hs over the ocean surface compared to Sentinel-3 SRAL and Jason-3 measurements during the fist 2-weeks of data aquisition.

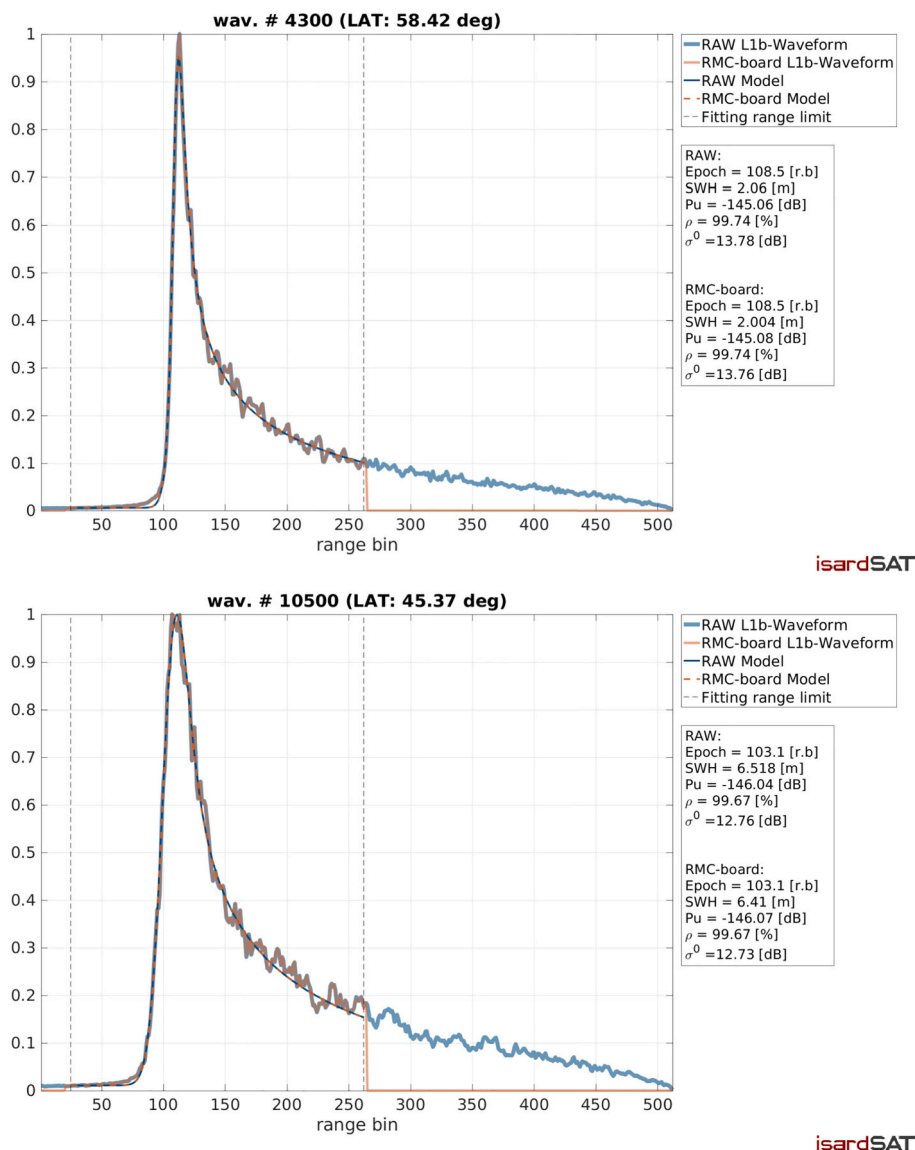Fig. 16 shows a comparison between data processed using the on

Fig. 16. Example waveforms from S6-MF obtained during the 30 November 2020 Poseidon-4 switch-on highlighting initial measurement performance. Top: Example for Hs = 2 m, Bottom: Example for Hs = 6 m. RAW SAR data were processed on the ground using the ESA Ground Prototype Processor (GPP) and show that the on-board RMC processor is performing within expectations.

board S6-MF RMC algorithm (orange line) and full resolution raw data processed by the ESA GPP on the ground (blue line). The low noise performance of the altimeter is notable. For both low and moderate sea state there are no significant differences in geophysical parameter retrieval performance between raw and RMC data processed on board. These results indicate that the processor on-board the satellite implementing the Range Migration Compensation (RMC) algorithm is functioning with expected performance.

Fig. 17(a) shows a Copernicus Sentinel-2 (ESA, 2012) colour composite image of the Ozero Nayval peninsula, Russia at a 10-m resolution on 29 October 2020. The peninsula is surrounded by a mountainous region and lies on the eastern part of the Bering Strait. It has a unique low-lying land-bound lagoon, various river and lake features that are clearly visible in the image that are marked together with the ground track of S6MF as it crosses the region. Fig. 17(b) shows a Copernicus Sentinel-1B (ESA, 2012) interferometric wide swath C-band radar image captured on 29 November 2020 that has been processed to 10 m resolution. The radar look direction is from the right with layover effects seen on the mountainous region to the left of the image. The lagoon has frozen over and numerous cracks are visible in the ice. Ocean swell and wind sea roughness are also seen in the ocean with some wave reflection and refraction on the southern coastal areas.

Fig. 17(c) shows a Poseidon-4 fully-focused SAR (FFSAR) image of the same area that reveals features of the Ozero Nayvak peninsular in fine detail. The high performance and low noise of Poseidon-4 enables this exceptional result. In this example, the altimeter data were first processed at a resolution of 1.1 m in the azimuth direction (left to right) and < 0.4 m in the range direction (vertical). Data are then multi-looked in azimuth to reduce speckle noise resulting in an image at a resolution of ~ 30 m. The radar backscatter power is coded by colour as a function of across-track range and clearly reveals features of sea ice in the lagoon and low-lying river and lake features. Unlike the Sentinel-1 image, the Sentinel-6 Poseidon-4 radar is illuminating the scene from top to bottom of the image and in this case, ocean wave structure and wave refraction at the southern coastline can be clearly seen. Unavoidable range ambiguities are seen in the upper part of the image. The low noise performance of Poseidon-4 measurements are clearly revealed in this striking result. Further work is required to explore this capability in marginal ice regions, over river and lake targets, and potentially for large ocean swell.

Compared to the moving ocean surface, static ground-based

reference transponders allow a detailed validation of σ^0, range, datation, and the point target response among other parameters. As part of the ESA Permanent Facility for Altimeter Calibration (PFAC) located in Crete, Greece (Mertikas et al., 2018, Mertikas et al., 2019a, Mertikas et al., 2019b, Mertikas et al., 2020), a transponder has been established in a mountainous area of western Crete (CDN1) as a dedicated external calibration source for satellite altimetry (Pavlis et al., 2004, Mertikas, 2010c; Mertikas et al., 2010a,b, Mertikas et al., 2011). the transponder is supported with in-situ reference systems (DORIS ground station, GNSS reference points, radiometer for wet tropospheric correction, etc. (Mertikas et al., 2020). The ESA PFAC is run operationally and maintains a complete uncertainty budget (Mertikas et al., 2019b) to Fiducial Reference Measurement (FRM, Donlon et al., 2015, Hollmann et al., 2013, BIPM, 1995; JCGM, 2008) quality.

Fig. 18 shows the results from the first PFAC transponder pass obtained on 18th December 2020 almost immediately after the tandem orbit configuration was acquired. Measurements have been corrected for wet and dry troposphere path delay using in situ radiometer and GPS measurements at the PFAC, and for solid earth tides. The CDN1 transponder exhibits an asymmetrical range response with an elevated first side-lobe associated with the transponder antenna gain pattern. This is of no concern since the same feature is also visible in all previous passes of Sentinel-3A, Sentinel-3B, CryoSat and Jason transponder measurements. Otherwise, the transponder results reveal a very symmetrical point target response in both range and azimuth that is well-centred and a range and azimuth resolution within expectations. Based on the preliminary results obtained from four independent analysis teams using three transponder passes between 18 December 2020 and 06 January 2021 we find a range difference of ~ 1 cm between S6-MF and Jason-3 that is consistent with a limited analysis of along-track SSH over the open ocean. For fully focussed SAR, we estimate a datation bias of ~ 10 μs ± 10 μs, an altimeter range noise of ~ 0.2 cm, a range resolution of 0.41 m (that is almost identical to the theoretical expectation) and an azimuth resolution of ~ 0.6 m. Further transponder passes will confirm these preliminary results.

Fig. 19 shows Copernicus Sentinel-6 sea-level anomaly data, overlaid on a map showing similar products from Jason-3, Sentinel-3A and Sentinel-3B. The background image is a map of sea-level anomalies from satellite altimeter data provided by the Copernicus Marine Environment Monitoring Service for 4 December 2020. The data for this image were taken from the Sentinel-6 'Short Time Critical Level 2 Low Resolution'
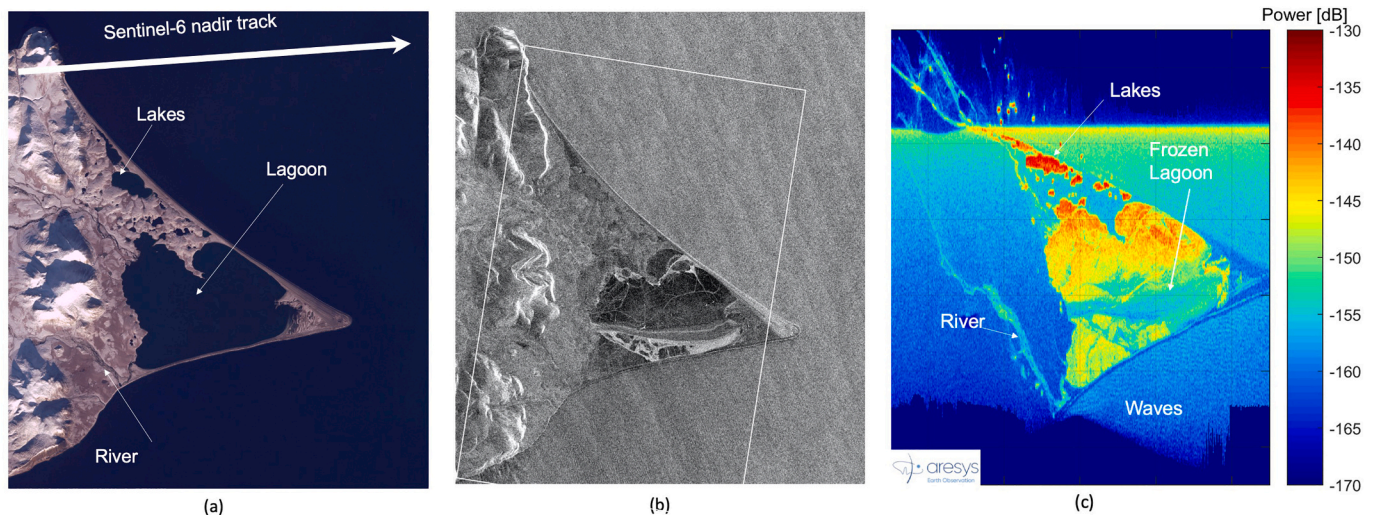

Fig. 17. (a) Sentinel-2B colour composite image of Ozero Nayvak peninsular (64.433 N, −172.3466 W), Russia obtained on 15th August 2020 with annotations of key features. (b) Sentinel-1b interferometric wide-swath C-band SAR image obtained on 29th November 2020. (c) S6-MF fully-focussed SAR (FFSAR) image obtained on November 30th 2020 processed by Aresys. The FFSAR image is not geolocated or projected and the white square indicates the approximate position of the Sentinel-6 altimeter image in (c).
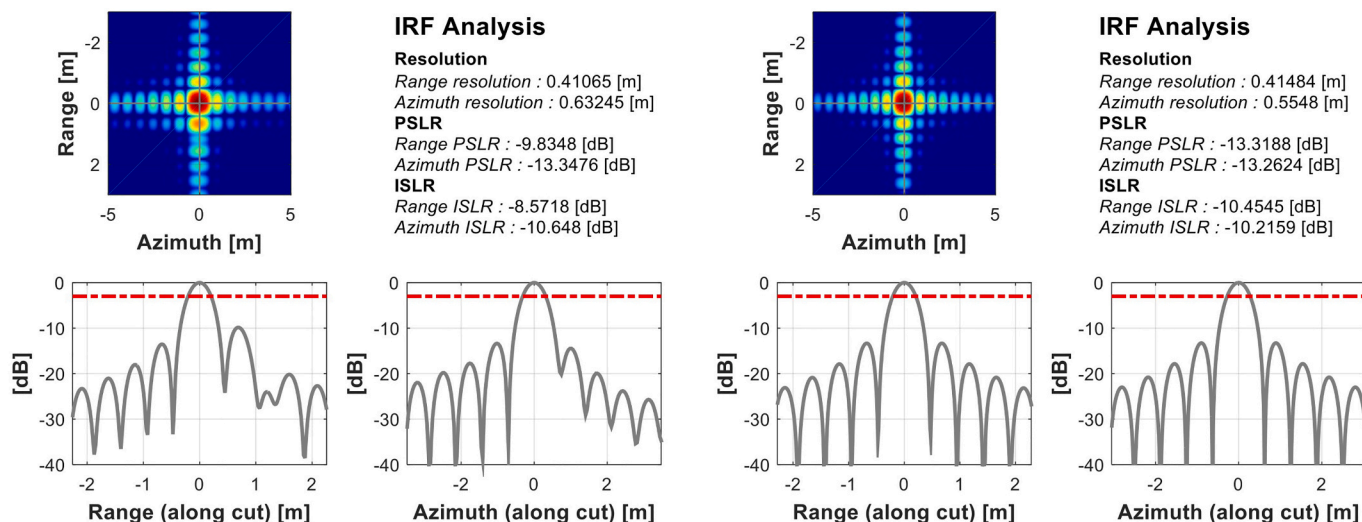
Fig. 18. (Left) Fully focussed SAR results from Posiedon-4 for the first PFAC transponder pass obtained on 18th November 2020 immediately after the S6MF tandem orbit configuration was acquired. Right: expected theoretical response. The asymmetry seen in the range cut is a feature of the PFAC transponder seen by all satellite measurments when using this system. Data processed by the ESA Ground Prototype Processor (GPP).
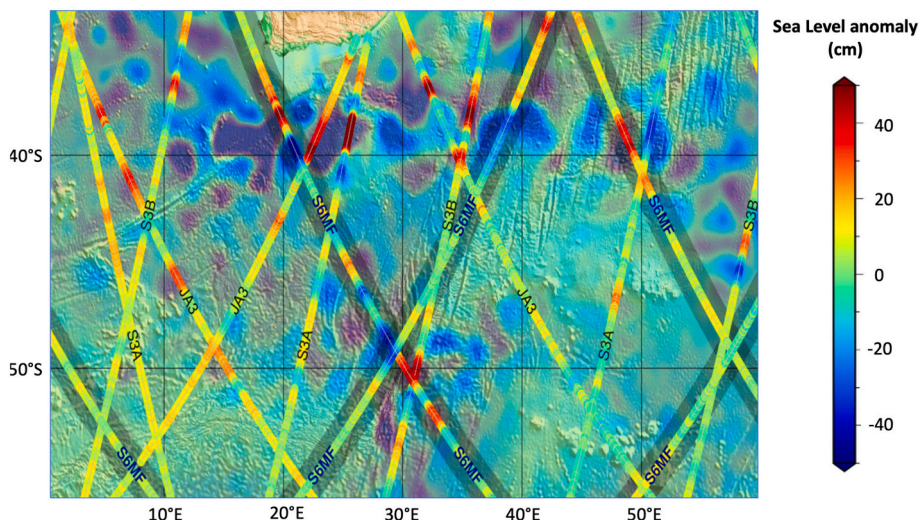

Fig. 19. Copernicus Sentinel-6 sea-level anomaly data, overlaid on a map showing similar products from Jason-3, Sentinel-3A and Sentinel-3B.The background image is a map of sea-level anomalies from satellite altimeter data provided by the Copernicus Marine Environment Monitoring Service for 4 December 2020. The S6-MF and Sentinel-3 tracks are from 5th December 2020.

products generated on 5 December. The Sentinel-3 track data were also acquired on 5th December 2020. A good consistency of measurement with Sentinel-3 and Jason-3 is evident.

After switch-on, the AMR-C and HRMR have been continuously acquiring data and global TB have been produced from all channels using pre-launch calibration. Instruments temperatures stabilised in the first day and both instruments are performing nominally. The preliminary early orbit performance of both AMR-C and HRMR is excellent: instrument diagnostics align with pre-launch values for gain, noise diode ratios, and noise equivalent difference temperature (NEΔT). Preliminary HRMR measurements show expected features over the globe with good water vapour dependence increasing with frequency and a higher sensitivity to snow cover over land. For AMR—C, TB are within about ~1% of on-Earth references using pre-launch calibration that is within the expected pre-launch uncertainty. The final AMR/HRMR calibration coefficients will be updated after SCS calibration results from the first cycles have been analysed. Fig. 20 shows the first cycle wet tropospheric path delay from S6-MF AMR-C using pre-launch calibration parameters with good qualitative agreement with Jason-3 path delays for same time

frame. Both AMR-C and HRMR are performing within expectation.

Fig. 21 shows the results obtained from the first SCS motion that was completed on 2nd December 2020 using a diagnostic mode in which only 18 and 23 GHz channels are available. Radiometric data show nominal performance with little to no gradient between SCS warm load temperatures and the SCS is performing within expectation. The AMR-C calibration is 0.2% relative to SCS target brightness temperature. Further analysis will refine these results using SCS calibration data to be performed every five days.

Building on these early results, the challenge is to confidently connect Sentinel-6 with the historical reference time series by detecting, characterising and mitigating errors, end-to-end biases and drifts. During the first 6–12 months after launch, the majority of ground-processing algorithms and all critical output quantities and associated errors will be calibrated and validated (ESA, 2020). A multi-national scientific activity will then continue throughout the mission lifetime to evolve the performance of the operational system to FRM standards. To coordinate Sentinel-6 international validation activities a Sentinel-6 Validation Team (S6VT) has been established (see http://www.s6vt.org for more
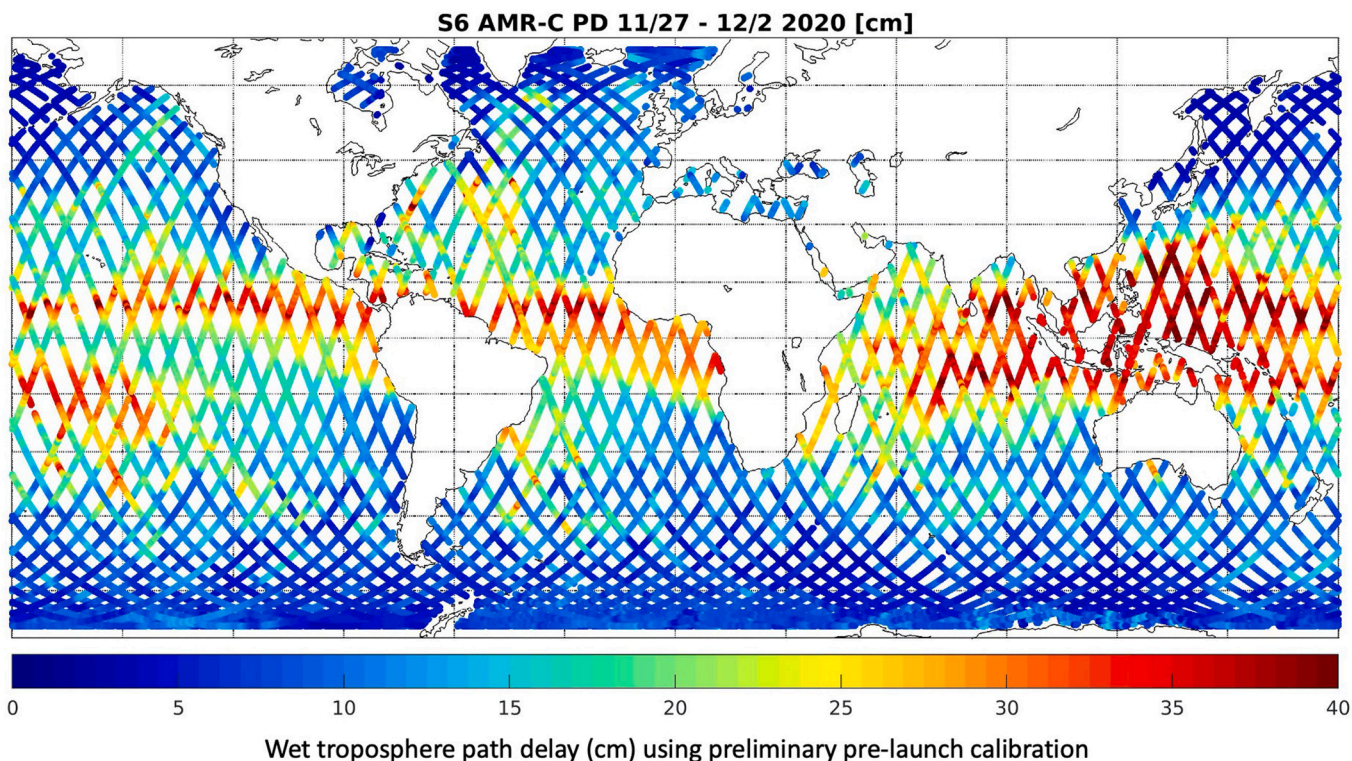
Fig. 20. The first cycle S6-MF AMR-C preliminary wet tropospheric path delay using pre-launch calibration. The final AMR/HRMR calibration coefficients will be updated after SCS calibration results have been analysed.

information). The core activities include statistical analysis of comparisons with other satellite missions based on established approaches (e.g. Scharroo et al., 2004, Ablain et al., 2010), external measurements from in-situ measurements (e.g. Mitchum, 1998, Bonnefond et al., 2011, 2018, Bonnefond et al., 2019, Watson et al., 2011, Chambers et al., 2003, Valladeau et al., 2012, Fu and Haines, 2013, Haines et al., 2010, 2020) and ground-based transponders (e.g. Mertikas et al., 2018, Mertikas et al., 2020). However, some elements such as instrument drift will require a much longer period that could extend to the mission lifetime (e.g. Cancet et al., 2013).

Fig. 21. Antenna Temperature (TA) results obtained from the first AMR-C SCS motion that was completed on 2nd December 2020 using a diagnostic mode in which only 18 and 23 GHz channels are available.

11. Summary and conclusion

The Copernicus Sentinel-6 Mission has been designed to continue the heritage satellite altimeter missions occupying the specific 'reference orbit' that have supplied the long-term reference data set to accurately monitor Mean Sea Level change that is recognised as a key indicator of climate change. Sentinel-6 mission is designed to address the needs of the European Copernicus programme for precise sea level, near-real-time measurements of sea surface height, significant wave height, and other products tailored to operational services in the climate, ocean, meteorology and hydrology domains. The mission is implemented through a unique international partnership with contributions from NASA, NOAA, ESA, EUMETSAT, and the European Union (EU). It includes two satellites that will fly sequentially (separated in time by 5 years). The first satellite, named Sentinel-6 Michael Freilich, was launched from Vandenburg Air Force Base, USA on 21st November 2020. The Poseidon-4 dual frequency (C/Ku-band) nadir-pointing radar altimeter provides synthetic aperture radar (SAR) processing in Ku-band to improve the signal through better along-track sampling and reduced measurement noise. It includes an innovative interleaved mode enabling radar data processing on two parallel chains, one with the SAR enhancements and the other furnishing a Low Resolution Mode that is fully backward-compatible with the historical T/P and Jason measurements. This allows a complete inter-calibration between the state-of-the-art data and the historical record. A three-channel Advanced Microwave Radiometer for Climate (AMR—C) provides measurements of atmospheric water vapour that would otherwise degrade the radar altimeter measurements. An experimental High Resolution Microwave Radiometer (HRMR) is also included in the AMR-C design to support improved performance in coastal areas. Additional sensors are included in the payload to provide Precise Orbit Determination, atmospheric sounding via GNSS-Radio Occultation and radiation monitoring around the spacecraft. Preliminary in-orbit performance data from Sentinel-6 Michael Freilich are presented and show the primary mission payload
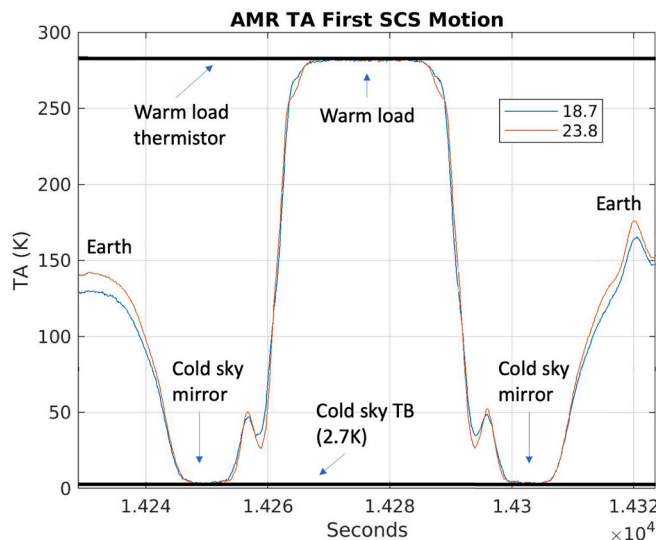
to be in line with expected performances. Following commissioning and tandem-flight operations, the Sentinel-6 mission will become the reference satellite altimeter providing unique evidence of sea level rise in support of European and International climate policy implementation and monitoring.

Credit author statement

Craig. J. Donlon: Writing of original manuscript, edits, revisions and figures.

Robert Cullen: writing/figure contributions to original manuscript.

Luisella Giulicchi: writing/figure contributions to original manuscript.

Pierrik Vuilleumier: writing contributions to original manuscript.

C. Richard Francis: writing contributions to original manuscript.

Mieke Kuschnerus: writing/figure contributions to original manuscript.

William Simpson: review and comments to manuscript.

Abderrazak Bouridah: contributions to original manuscript.

Mauro Caleno: review and comments to manuscript.

Roberta Bertoni: review and comments to manuscript.

Jesus Rancaño: review and comments to manuscript.

Eric Pourier: review and comments to manuscript.

Andrew Hyslop: review and comments to manuscript.

James Mulcahy: review and comments to manuscript.

Robert Knockaert: review and comments to manuscript.

Christopher Hunter: review and comments to manuscript.

Alan Webb: review and comments to manuscript.

Marco Fornari: writing/figure contributions to original manuscript uscript.

Parag Vaze: supervision of JPL team.

Shannon Brown: writing/figure contributions to original manuscript.

Joshua Willis: review and comments to manuscript.

Shailen Desai: review and comments to manuscript.

Jean-Damien Desjonqueres: review and comments to manuscript.

Remko Scharroo: writing/figure contributions to original manuscript.

Cristina Martin-Puig: review and comments to manuscript.

Eric Leuliette: review and comments to manuscript.

Alejandro Egido: writing contributions to original manuscript.

Walter H. F. Smith: writing/figure contributions to original manuscript.

Pascal Bonnefond:: review and comments to manuscript.

Sophie Le Gac: writing/figure contributions to original manuscript.

Nicolas Picot: review and comments to manuscript.

and Gilles Tavener: review and comments to manuscript.

Declaration of Competing Interest

The authors declare that they have no known competing financial interests or personal relationships that could have appeared to influence the work reported in this paper.

Acknowledgements

References

Abdalla, S., 2012. Ku-band radar altimeter surface wind speed algorithm. Mar. Geod. 35 (sup1), 276–298. https://doi.org/10.1080/01490419.2012.718676.

Ablain, M., Dorandeu, J., Le Traon, P.-Y., Sladen, A., 2006. High resolution altimetry reveals new characteristics of the December 2004 Indian Ocean tsunami. Geophys. Res. Lett. 33, L21602 https://doi.org/10.1029/2006GL027533.

Ablain, M., Cazenave, A., Valladeau, G., Guinehut, S., 2009. A new assessment of the error budget of global mean sea level rate esti- mated by satellite altimetry over 1993–2008. Ocean Sci. 5, 193–201. https://doi.org/10.5194/os-5-193-2009.

Ablain, M., Philipps, S., Picot, N., Bronner, E., 2010. Jason-2 global statistical assessment and cross-calibration with Jason-1. Mar. Geod. 33 (S1), 162–185. https://doi.org/10.1080/01490419.2010.487805.

Ablain, M., Cazenave, A., Larnicol, G., Balmaseda, M., Cipollini, P., Faugère, Y., Fernandes, M.J., Henry, O., Johannessen, J.A., Knudsen, P., Andersen, O., Legeais, J., Meyssignac, B., Picot, N., Roca, M., Rudenko, S., Scharffenberg, M.G., Stammer, D., Timms, G., Benveniste, J., 2015. Improved sea level record over the satellite altimetry era (1993–2010) from the Climate Change Initiative project. Ocean Sci. 11, 67–82. https://doi.org/10.5194/os-11-67-2015, 2015.

Ablain, M., Meyssignac, B., Zawadzki, L., Jugier, R., Ribes, A., Spada, G., Benveniste, J., Cazenave, A., Picot, N., 2019. Uncertainty in satellite estimates of global mean sea-level changes, trend and acceleration. Earth Syst. Sci. Data 11, 1189–1202. https://doi.org/10.5194/essd-11-1189-2019, 2019.

Alves, J.H.G.M., Young, I.R., 2004. On estimating extreme wave heights using combined Geosat, TOPEX/Poseidon and ERS-1 altimeter data. Appl. Ocean Res. 25 (4), 167–186.

Anthes, R.A., Bernhardt, P.A., Chen, Y., Cucurull, L., Dymond, K.F., Ector, D., Healy, S.B., Ho, S.-P., Hunt, D.C., Kuo, Y.-H., Liu, H., Manning, K., McCormick, C., Meehan, T.K., Randel, W.J., Rocken, C., Schreiner, W.S., Sokolovskiy, S.V., Syndergaard, S., Thompson, D.C., Trenberth, K.E., Wee, T.-K., Yen, N.L., Zeng, Z., 2008. The COSMIC/FORMOSAT-3 mission: early results. Bull. Am. Meteorol. Soc. 89, 313–333.

Ardhuin, F., Stopa, J.E., Chapron, B., Collard, F., Husson, R., Jensen, R., Johannessen, J., Mouche, A., Pasaro, M., Quartly, G., Swail, V., Young, I., 2019. Observing sea states. Front. Mar. Sci. 6 https://doi.org/10.3389/fmars.2019.00124, 124-.

Auriol, A., Tourain, C., 2010. DORIS system: the new age, in DORIS special issue: precise orbit determination and applications to the earth sciences, P. Willis (Ed.). Adv. Space Res. 46 (12), 1484–1496. https://doi.org/10.1016/j.asr.2010.05.015.

Beckley, B.D., Callahan, P.S., Hancock, D.W., Mitchum, G.T., Ray, R.D., 2017. On the 'Cal-Mode' correction to TOPEX satellite altimetry and Its effect on the global mean sea level time series. J. Geophys. Res. C: Oceans 122 (11), 8371–8384. https://doi.org/10.1002/2017jc013090.

Bidlot, J.R., 2017. Twenty-one years of wave forecast verification. ECMWF Newslett. 150, 31–36.

BIPM, 1995. Comptes rendus de la 20e reunion de la Conference generale des poids et mesures. Available online at. http://www.bipm.org/en/CGPM/db/20/S.

Bloßfeld, M., Zeitlhöfler, J., Rudenko, S., Dettmering, D., 2020. Observation-based attitude realization for accurate Jason satellite orbits and its impact on geodetic and altimetry results. Remote Sens. 2020 (12), 682.

Bonnefond, P., Haines, B.J., Watson, C., 2011. In Situ Absolute Calibration and Validation: A Link from Coastal to Open-Ocean Altimetry. Springer, pp. 259–296. https://doi.org/10.1007/978-3-642-12796-0_11. Berlin Heidelberg, Berlin, Heidelberg. chapter 11.

Bonnefond, P., Laurain, O., Exertier, P., Boy, F., Guinle, T., Picot, N., Labroue, S., Raynal, M., Donlon, C., Féménias, P., Parrinello, T., Dinardo, S., 2018. Calibrating the SAR SSH of sentinel-3A and CryoSat-2 over the Corsica facilities. Remote Sens. 2018 (10), 92.

Bonnefond, P., Exertier, P., Laurain, O., Guinle, T., Féménias, P., 2019. Corsica: A 20-Yr Multi-Mission Absolute Altimeter Calibration Site, Advances in Space Research, Special Issue « 25 Years of Progress in Radar Altimetry » https://doi.org/10.1016/j.asr.2019.09.049.

Boy, F., Desjonqueres, J.D., Picot, N., Moreau, T., Raynal, M., 2016. CryoSat-2 SAR-mode over oceans: processing methods, global assessment, and benefits. IEEE Trans. Geosci. Remote Sens. 2016 (55), 148–158.

Brown, G.S., 1977. The average impulse response of a rough surface and its applications. IEEE Trans. Antennas Propag. 25 (1), 67–74.

Brown, S., 2006. AMR Beam Matching Algorithm, JPL Technical Document (12 October 2006).

Brown, S., 2013. Maintaining the long-term calibration of the Jason-2/OSTM advanced microwave radiometer through intersatellite calibration. IEEE Trans. Geosci. Remote Sens. 51 (3), 1531–1543. March 2013. https://doi.org/10.1109/TGRS.2012.2213262.

Brown, S., Ruf, C., Keihm, S., Kitiyakara, A., 2004. Jason microwave radiometer performance and on-orbit calibration. Mar. Geod. 27 (1–2), 199–220.

Brown, S., Desai, S., Keihm, S., Lu, W., 2009. Microwave radiometer calibration on decadal time scales using on-earth brightness temperature references: application to the TOPEX microwave radiometer. J. Atmos. Ocean. Technol. 26, 2579–2591.

Buontempo, C., Hutjes, R., Beavis, P., Berckmans, J., Cagnazzo, C., Vamborg, F., Thépaut, J.-N., Bergeron, C., Almond, S., Amici, A., Ramasamy, S., Dee, D., 2020. Fostering the development of climate services through Copernicus Climate Change Service (C3S) for agriculture applications. Weather Climate Extremes 27. https://doi.org/10.1016/j.wace.2019.100226.

Bushair, M.T., Gairola, R.M., 2019. A combined passive–active microwave retrieval of ocean surface wind speed from SARAL-AltiKa microwave radar altimeter and radiometer. Meteorog. Atmos. Phys. 131, 1205–1212. https://doi.org/10.1007/s00703-018-0631-4.

Camargo, C.M.L., Riva, R.E.M., Hermans, T.H.J., Slangen, A.B.A., 2020. Exploring sources of uncertainty in steric sea-level change estimates. J. Geophys. Res. Oceans 125. https://doi.org/10.1029/2020JC016551 e2020JC016551.

Campos, R.M., Alves, J.G., Penny, S.G., et al., 2020. Global assessments of the NCEP ensemble forecast system using altimeter data. Ocean Dyn. 70, 405–419. https://doi.org/10.1007/s10236-019-01329-4.

Cancet, M., Bijac, S., Chimot, J., Bonnefond, P., Jeansou, E., Laurain, O., Lyard, F., Bronner, E., Fémenias, P., 2013. Regional in situ validation of satellite altimeters: Calibration and cross-calibration results at the Corsican sites. Adv. Space Res. 51 (8), 1400–1417, 15 April 2013. ISSN 0273-1177. https://doi.org/10.1016/j.asr.2012.06.017.

Carrere, L., Arbic, B.K., Dushaw, B., Egbert, G.D., Erofeeva, S.Y., Lyard, F., Ray, R.D., Ubelmann, C., Zaron, E., Zhao, Z., Shriver, J.F., Buijsman, M.C., Picot, N., 2020. Accuracy assessment of global internal tide models using satellite altimetry. Ocean Sci. Discuss. https://doi.org/10.5194/os-2020-57 (in review).

Cazenave, A., Palanisamy, H., Ablain, M., 2018. Contemporary sea level changes from satellite altimetry: what have we learned? What are the new challenges? Adv. Space Res. 62, 1639–1653. https://doi.org/10.1016/j.asr.2018.07.017.

Chambers, D.P., Ries, J.C., Urban, T.J., 2003. Calibration and verification of Jason-1 using global along-track residuals with TOPEX. Mar. Geod. 26 (3&4), 305–317. https://doi.org/10.1080/714044523.

Chelton, D.B., Schlax, M.G., Samelson, R.M., de Szoeke, R.A., 2007. Global observations of large oceanic eddies. Geophys. Res. Lett. 34, L15606 https://doi.org/10.1029/2007GL030812.

Chen, X., et al., 2017. The increasing rate of global mean sea-level rise during 1993–2014. Nat. Clim. Chang. 7, 492–495.

Cheng, L., Abraham, J., Trenberth, K.E., et al., 2021. Upper ocean temperatures hit record high in 2020. Adv. Atmos. Sci. 2021 https://doi.org/10.1007/s00376-021-0447-x.

Clerc, S., Donlon, C., Borde, F., Lamquin, N., Hunt, S.E., Smith, D., McMillan, M., Mittaz, J., Woolliams, E., Hammond, M., Banks, C., Moreau, T., Picard, B., Raynal, M., Rieu, P., Guérou, T., 2020. A. Benefits and lessons learned from the sentinel-3 tandem phase. Remote Sens. 12, 2668, 2020.

Climate Change Initiative Coastal Sea Level Team, 2020. Coastal sea level anomalies and associated trends from Jason satellite altimetry over 2002-2018. Scientific Data 7 (1), 357. https://doi.org/10.1038/s41597-020-00694-w.

CNES, 2006. OSTM/Jason-2 science and operational requirements, TP3-J0-SP-188-CNES Mar 6, 2006 available from CENTRE NATIONAL D'ÉTUDES SPATIALES. Toulouse, France.

Cooper, C.K., Forristall, G.Z., 1997. The use of satellite altimeter data to estimate extreme wave climate. J. Atmos. Ocean. Technol. 14 (2), 254–266.

Couderc, V., 2015. Jason-3 system requirements document, TP4-J0-STB-44-CNES v 1.3, Centre Nationale d'Etudes Spatiales, Toulouse, 2015. CNES.

Cullen, R., Davidson, M.W.J., Drinkwater, M.R., Francis, C.R., Haas, C., Hawley, R.L., Mavrocordatos, C.M., Morris, E.M., Rack, W., Ratier, G., Viau, P., Wingham, D.J., 2006. 'ESA's new range of radar altimeters for the extraction of geophysical parameters from land, sea ice and ocean surfaces' Proc. Radar Altimeter Symposium, Venice March 2006.

Desorgher, L., et al., 2013. ESA Next Generation Radiation Monitor, 14th European Conference on Radiation and Its Effects on Components and Systems (RADECS), Oxford, 2013, pp. 1–5. https://doi.org/10.1109/RADECS.2013.6937362.

Desportes, C., Obligis, E., Eymard, L., 2007. On the wet tropospheric correction for altimetry in coastal regions. IEEE Trans. Geosci. Rem. Sens. 45 (7), 2139–2149.

Dibarboure, G., Boy, F., Desjonqueres, J.D., Labroue, S., Lasne, Y., Picot, N., Poisson, J. C., Thibaut, P., 2014. Investigating short-wavelength correlated errors on low-resolution mode altimetry. J. Atmos. Ocean. Technol. 31, 1337–1362. https://doi.org/10.1175/JTECH-D-13-00081.1.

Dieng, H., Cazenave, A., Meyssignac, B., Ablain, M., 2017. New estimate of the current rate of sea level rise from a sea level budget approach. Geophys. Res. Lett. 44 https://doi.org/10.1002/2017GL073308.

Dodet, G., Piolle, J.-F., Quilfen, Y., Abdalla, S., Accensi, M., Ardhuin, F., Ash, E., Bidlot, J.-R., Gommenginger, C., Marechal, G., Pasesaro, M., Quartly, G., Stopa, J., Timmermans, B., Young, I., Cipollini, P., Donlon, C., 2020. The Sea State CCI dataset v1: towards a sea state climate data record based on satellite observations. Earth Syst. Sci. Data 12, 1929–1951. https://doi.org/10.5194/essd-12-1929-2020, 2020.

Donlon, C., 2011. Sentinel-3 Mission Requirements Traceability Document (MRTD), EOP-SM/2184/CD-cd, v1.0, European Space Agency, Noordwijk, the Netherlands.

Donlon, C., Berruti, B., Buongiorno, A., Ferreira, M.-H., Fémenias, P., Frerick, J., Goryl, P., Klein, U., Laur, H., Mavrocordatos, C., Nieke, J., Rebhan, H., Seitz, B., Stroede, J., Sciarra, R., 2012. The global monitoring for environment and security (GMES) sentinel-3 mission. Remote Sens. Environ. 120, 37–57.

Donlon, C.J., Minnett, P., Fox, N., Wimmer, W., 2015. Strategies for the laboratory and field deployment of ship-borne fiducial reference thermal infrared radiometers in support of satellite-derived sea surface temperature climate data records. In: Zibordi, G., Donlon, C., Parr, A. (Eds.), 2015. Optical Radiometry for Oceans Climate Measurements, Vol. 47 Experimental Methods in Sciences. Elsevier, ISBN 9780124170117, 697 pp.

Donlon, C., Scharroo, R., Willis, J., Leuliette, E., Bonnefond, P., Picot, N., Schrama, E., Brown, S., 2019. Sentinel-6A/B/Jason-3 Tandem Phase Configurations, JC-TN-ESA-MI-0876 V2.0, 8 July 2019, available from the European space agency, Noordwijk, the Netherlands.

Dorandeu, J., Ablain, M., Le Traon, P.-Y., 2003. Reducing cross- track geoid gradient errors around TOPEX/Poseidon and Jason-1 nominal tracks: application to calculation of sea level anomalies. J. Atmos. Ocean. Technol. 20, 1826–1838.

Ducet, N., Le Traon, P.Y., Reverdin, G., 2000. Global high-resolution mapping of ocean circulation from TOPEX/Poseidon and ERS-1 and 2. J. Geophys. Res. 105, 9,477–19,498.

Egido, A., Smith, W.H.F., 2019. Pulse-to-pulse correlation effects in high PRF low-resolution mode altimeters. IEEE Trans. Geosci. Remote Sens. 2019 (57), 2610–2617.

Emery, C.M., Paris, A., Biancamaria, S., Boone, A., Calmant, S., Garambois, P.-A., Santos da Silva, J., 2018. Large-scale hydrological model river storage and discharge correction using a satellite altimetry-based discharge product. Hydrol. Earth Syst. Sci. 22, 2135–2162. https://doi.org/10.5194/hess-22-2135-2018, 2018.

ESA, 2012. Sentinel-2: ESA's Optical High-Resolution Mission for GMES Operational Services, (ESA SP-1322/2 March 2012) available from ESA/ESTEC. Noordwijk, The Netherlands.

ESA, 2012. Sentinel-1: ESA's Radar Observatory Mission for GMES Operational Services (ESA SP-1322/1, March 2012). ESA, 978-92-9221-418-0.

ESA, 2018. Jason CS/Sentinel 6 analysis of on-board RMC processing, JC-TN-ESA-MI-0769, v1 rev. 2 August 2018, available from European Space Agency, Noordwijk, the Netherlands. ESA.

ESA, 2020. Sentinel-6 Mission Performance Working Group cal/val concept Plan, JC-TN-ESA-MI-0500, available from ESA/ESTEC Noordwijk, the Netherlands.

Escudier, P., Fellous, J.-L., 2008. The Next 15 Years of Satellite Altimetry Ocean Surface Topography Constellation, User Requirements Document. CEOS available from. http://ceos.org/observations/documents/Satellite_Altimetry_Report_2009-10.pdf.

EU, 2014. Regulation (EU) No 377/2014 of the European Parliament and of the Council of 3 April 2014 establishing the Copernicus Programme and repealing Regulation (EU) No 911/2010 Text with EEA relevance. available from. https://eur-lex.europa.eu/legal-content/EN/TXT/?uri=CELEX%3A32014R0377.

Fernandes, M.J., Lázaro, C., Ablain, M., Pires, N., 2015. Improved wet path delayPDs for all ESA and reference altimetric missions. Remote Sens. Environ. 169, 50–74. https://doi.org/10.1016/j.rse.2015.07.023.

Fernandez, J., Escobar, D., Ayuga, F., et al., 2015. Copernicus POD service operations. In: Proceedings of the Sentinel-3 for Science Workshop, 2–5 June 2015, Venice, Italy, (ESA SP-734). ESA Communications, ESTEC, Noordwijk, The Netherlands.

Francis, C.R., 2002. Design of the CryoSat system. In: *IEEE International Geoscience and Remote Sensing Symposium*, Toronto, Ontario, Canada, 2002, vol.3, pp. 1759–1761. https://doi.org/10.1109/IGARSS.2002.1026245.

Frew, N., Glover, M., Bock, D.M., McCue, S.J., 2007. A new approach to estimation of global air-sea gas transfer velocity fields using dual-frequency altimeter backscatter. J. Geophys. Res. 112, C11003 https://doi.org/10.1029/2006JC003819.

Fu, L., Haines, B.J., 2013. The challenges in long-term altimetry calibration for addressing the problem of global sea level change. Adv. Space Res. 51, 1284–1300, 2013.

Fu, L.-L., Christensen, E.J., Yamarone, C.A., Lefebvre, M., Ménard, Y., Dorrer, M., Escudier, P., 1994. TOPEX/POSEIDON mission overview. J. Geophys. Res. 99 (C12), 24369–24381. https://doi.org/10.1029/94JC01761.

Gao, Q., Makhoul, E., Escorihuela, M.J., Zribi, M., Segui, P.Q., Garcia, P., Roca, M., 2019. Analysis of retrackers' performances and water level retrieval over the Ebro River basin using sentinel-3. Remote Sens. 11 (6), 718. https://doi.org/10.3390/rs11060718.

Garbe, J., Albrecht, T., Levermann, A., et al., 2020. The hysteresis of the Antarctic ice sheet. Nature 585, 538–544. https://doi.org/10.1038/s41586-020-2727-5.

GCOS, 2011. Systematic observation requirements for satellite-based data products for climate, 2011 Update. Supplemental details to the satellite-based component of the "Implementation Plan for the Global Observing System for Climate in Support of the UNFCCC (2010 Update)", United Nations Environment Programme, International Council For Science, December 2011 GCOS – 154.

GCOS, 2016. GCOS Implementation Plan, p. 2016 available from. http://www.wmo.int/pages/prog/gcos/index.php.

Goddijn-Murphy, L., Woolf, D.K., Chapron, B., Queffeulou, P., 2013. Improvements to estimating the air–sea gas transfer velocity by using dual-frequency, altimeter backscatter. Remote Sens. Environ. 139, 1–5. https://doi.org/10.1016/j.rse.2013.07.026.

Gommenginger, C.P., Martin-Puig, C., Dinardo, S., Cotton, P.D., Benveniste, J., 2012. Improved Altimetric Performance of CryoSat-2 SAR Mode over the Open Ocean and the Coastal Zone, Presented at the European Geosciences Union General Assembly, Vienna, Austria, 22–27 April 2012, 2012.

Gommenginger, C.P., Martin-Puig, C., Amarouche, L., Raney, K., 2013a. SAR Mode Error Budget Study: Review of State of Knowledge of SAR Altimetry over Ocean, EUMETSAT Ref. EUM/RSP/REP/14/749304, version 2.2, Darmstadt, Germany, 2013.

Gommenginger, C., Martin-Puig, C.A., Laiba Raney, R.K., 2013b. Review of state of knowledge for SAR altimetry over ocean. Report of the EUMETSAT JASON-CS SAR

mode error budget study (EUMETSAT Reference, EUM/RSP/REP/14/749304, Version 2.2) Southampton, GB. National Oceanography Centre 57pp.

Haines, B., Desai, S., Born, G., 2010. The harvest experiment: calibration of the climate data record from TOPEX/Poseidon, Jason-1 and the Ocean Surface Topography Mission. Mar. Geod. 33 (Suppl. 1), 91–113. https://doi.org/10.1080/01490419.2010.491028, 2010.

Haines, B., Desai, S.D., Kubitschek, D., Leben, R.R., 2020. A brief history of the harvest experiment: 1989–2019. Adv. Space Res. URL: http://www.sciencedirect.com/science/article/pii/S0273117720305718, doi: 10.1016/j.asr.2020.08.013.

Halimi, A., Mailhes, C., Tourneret, J.-Y., Thibaut, P., Boy, F., 2014. A semi-analytical model for delay/Doppler altimetry and its estimation algorithm. IEEE Trans. Geosci. Rem. Sens. 52, 4248–4258. https://doi.org/10.1109/TGRS.2013.2280595, 2014.

Hamlington, B.D., Frederikse, T., Nerem, R.S., Fasullo, J.T., Adhikari, S., 2020. Investigating the acceleration of regional sea level rise during the satellite altimeter era. Geophys. Res. Lett. 47 https://doi.org/10.1029/2019GL086528 e2019GL086528.

Hanafin, J.A., Coauthors, 2012. Phenomenal sea states and swell from a North Atlantic Storm in February 2011: A comprehensive analysis. Bull. Amer. Meteor. Soc. 93, 1825–1832. https://doi.org/10.1175/BAMS-D-11-00128.1.

Healy, B., Polichtchouk, I., Horányi, A., 2020. Monthly and zonally averaged zonal wind information in the equatorial stratosphere provided by GNSS radio occultation. Q. J. R. Meteorol. Soc 1–10. https://doi.org/10.1002/qj.3870, 2020.

Hein, G.W., Pany, T., 2002. Architecture and signal design of the European satellite navigation system galileo – status Dec. 2002. J. Glob. Position. Syst. 1 (2), 73–84.

Ho, S.-P., Anthes, R.A., Ao, C.O., Healy, S.B., Horanyi, A., Hunt, D., Mannucci, A.J., Pedatella, N., Randel, W.J., Simmons, A., Steiner, A., Xie, F., Yue, X., Zeng, Z., 2019. The COSMIC/FORMOSAT-3 radio occultation mission after 12 years: accomplishments, remaining challenges, and potential impacts of COSMIC-2. Bull. Am. Meteor. Soc. https://doi.org/10.1175/BAMS-D-18-0290.1.

Hollmann, R., et al., 2013. The ESA climate change initiative: satellite data records for essential climate variables. Bull. Amer. Meteor. Soc. 94, 1541–1552. https://doi.org/10.1175/BAMS-D-11-00254.1, 2013.

Huess, V., Andersen, O.B., 2001. Seasonal variation in the main tidal constituent from altimetry. Geophys. Res. Lett. 28, 567–570. https://doi.org/10.1029/2000GL011921.

IPCC, 2014. Climate Change 2014: Synthesis Report. Contribution of Working Groups I, II and III to the Fifth Assessment Report of the Intergovernmental Panel on Climate Change [Core Writing Team, R.K. Pachauri and L.A. Meyer (eds.)]. 2014. IPCC, Geneva, Switzerland, 151 pp.

IPCC, 2019. IPCC Special Report on the Ocean and Cryosphere in a Changing Climate [H.-O. Pörtner, D.C. Roberts, V. Masson-Delmotte, P. Zhai, M. Tignor, E. Poloczanska, K. Mintenbeck, A. Alegría, M. Nicolai, A. Okem, J. Petzold, B. Rama, N. M. Weyer (eds.)], available online at. https://www.ipcc.ch/srocc/download-report/.

Jayles, C., Berthias J.-P., Laurichesse, D., Nordine, S., Cauquil, P., Tavernier, G., 2002. DORIS-DIODE: two-years results of the first European navigator. Adv. Space Res. 30 (2), 301–306. https://doi.org/10.1016/S0273-1177(02)00299-5.

Jayles, C., Nhun-Fat, B., Tourain, C., 2006. DORIS: system description and control of the signal integrity. J. Geod. 80, 457–472. https://doi.org/10.1007/s00190-006-0046-8.

Jayles, C., Chauveau, J.P., Didelot, F., Auriol, A., Tourain, C., 2016. DORIS system and integrity survey. Adv. Space Res. 58 (2016), 2691–2706. https://doi.org/10.1016/j.asr.2016.05.032.

JCGM, 2008. Evaluation of measurement data — Guide to the expression of uncertainty in measurement JCGM 100:2008, GUM 1995 with minor corrections, First edition September 2008. available from. http://www.bipm.org/utils/common/documents/jcgm/JCGM_100_2008_E.pdf.

Johnston, G., Riddell, A., Hausler, G., 2017. The international GNSS service. In: Teunissen, Peter, J.G., Montenbruck, O. (Eds.), Springer Handbook of Global Navigation Satellite Systems, first ed. Springer International Publishing, Cham, Switzerland, pp. 967–982. https://doi.org/10.1007/978-3-319-42928-1.

Kangaslahti, P., et al., 2019. High resolution microwave radiometer in AMR-C on sentinel-6. In: *Proc 6th Workshop Adv. RF Sensors Remote Sens. Instrum. 4th Ka-Band Earth Observ. Radar Missions Workshop*, Nov. 11–13, 2019, [online]. Available: https://atpi.eventsair.com/QuickEventWebsitePortal/arsikeo/website.

Keihm, S.J., Janssen, M.A., Ruf, C.S., 1995. TOPEX/POSEIDON microwave radiometer (TMR): III. Wet troposphere range correction algorithm and pre-launch error budget. IEEE Trans. Geosci. Remote Sens. 33, 147–161.

Kursinski, E.R., Hajj, G.A., Schofield, J.T., Linfield, R.P., Hardy, K.R., 1997. Observing Earth's atmosphere with radio occultation measurements using the Global Positioning System. J. Geophys. Res. 102, 23429–23465.

Lambin, J., Morrow, R., Fu, L.-L., Willis, J.K., Bonekamp, H., Lillibridge, J., Perbos, J., Zaouche, G., Vaze, P., Bannoura, W., Parisot, F., Thouvenot, E., Coutin-Faye, S., Lindstrom, E., Mignogno, M., 2010. The OSTM/Jason-2 mission. Mar. Geod. 33 (4–25), 2010. https://doi.org/10.1080/01490419.2010.491030.

Lambin, J., Morrow, R., Fu, L.-L., Willis, J.K., LEuliette, E., Lillibridge, L., Bonekamp, H., 2011. Jason-3 Mission Requirements Document, Issue 1, available from CNES. Toulouse, France.

Lázaro, C., Fernandes, M.J., Vieira, T., Vieira, E., 2019. A coastally improved global dataset of wet tropospheric corrections for satellite altimetry. Earth Syst. Sci. Data Discuss. https://doi.org/10.5194/essd-2019-171.

Le Gac, S., Boy, F., Blumstein, D., Lasson, L., Picot, N., 2019. Benefits of the open-loop tracking command (OLTC): extending conventional nadir altimetry to inland waters monitoring. Adv. Space Res. 2019.

Le Roy, Y., Deschaux-Beaume, M., Mavrocordatos, C., Borde, F., 2010. SRAL, A radar altimeter designed to measure a wide range of surface types, Geoscience and Remote Sensing Symposium, 2009 IEEE International, IGARSS 2009. IEEE International, IGARSS, pp. 445–448.

Le Traon, P.-Y., Antoine, D., Bentamy, A., Bonekamp, H., Breivik, L.A., Chapron, B., Corlett, G., Dibarboure, G., DiGiacomo, P., Donlon, C., Faugère, Y., Font, J., Girard-Ardhuin, F., Gohin, F., Johannessen, J.A., Kamachi, M., Lagerloef, G., Lambin, J., Larnicol, G., Le Borgne, P., Leuliette, E., Lindstrom, E., Martin, M.J., Maturi, E., Miller, L., Mingsen, L., Morrow, R., Reul, N., Rio, M.H., Roquet, H., Santoleri, R., Wilkin, J., 2015. Use of satellite observations for operational oceanography: recent achievements and future prospects. J. Oper Oceanogr. 8 (S1), 12–27.

Le Traon, P.-Y., Reppucci, A., Alvarez Fanjul, E., Aouf, L., Behrens, A., Belmonte, M., Bentamy, A., Bertino, L., Brando, V.E., Kreiner, M.B., Benkiran, M., Carval, T., Ciliberti, S.A., Claustre, H., Clementi, E., Coppini, G., Cossarini, G., De Alfonso, Alonso-Muñoyerro M., Delamarche, G., Dibarboure, G., Dinessen, F., Drevillon, M., Drillet, Y., Faugere, Y., Fernández, V., Fleming, A., Garcia-Hermosa, M.I., Sotillo, M.G., Garric, G., Gasparin, F., Giordan, C., Gehlen, M., Gregoire, M.L., Guinehut, S., Hamon, M., Harris, P., Hernandez, F., Hinkler, J.B., Hoyer, J., Karvonen, J., Kay, S., King, R., Lavergne, T., Lemieux-Dudon, B., Lima, L., Mao, C., Martin, M.J., Masina, S., Melet, A., Buongiorno Nardelli, B., Nolan, G., Pascual, A., Pistoia, J., Palazov, A., Piolle, J.F., Pujol, M.I., Pequignet, A.C., Peneva, E., Pérez Gómez, B., Petit de la Villeon, L., Pinardi, N., Pisano, A., Pouliquen, S., Reid, R., Remy, E., Santoleri, R., Siddorn, J., She, J., Staneva, J., Stoffelen, A., Tonani, M., Vandenbulcke, L., von Schuckmann, K., Volpe, G., Wettre, C., Zacharioudaki, A., 2019. From observation to information and users: the copernicus marine service perspective. Front. Mar. Sci. 6, 234. https://doi.org/10.3389/fmars.2019.00234.

Legeais, J.-F., Ablain, M., Zawadzki, L., Zuo, H., Johannessen, J.A., Scharffenberg, M.G., Fenoglio-Marc, L., Fernandes, M.J., Andersen, O.B., Rudenko, S., Cipollini, P., Quartly, G.D., Passaro, M., Cazenave, A., Benveniste, J., 2018. An improved and homogeneous annual mean sea level record from the ESA Climate Change Initiative. Earth Syst. Sci. Data 10, 281–301. https://doi.org/10.5194/essd-10-281-2018.

Leighton, T.G., Coles, D.G.H., Srokosz, M., White, P.R., Woolf, D.K., 2018. Asymmetric transfer of CO2 across a broken sea surface. Sci. Rep. 8, 8301. https://doi.org/10.1038/s41598-018-25818-6.

LeRoy, Deschaux-Beaume, Mavrocordatos, Borde, et al., 2009. SRAL, A radar altimeter designed to measure a wide range of surface types. IEEE International Geoscience and Remote Sensing Symposium, Cape Town, South Africa, 2009 445–448. https://doi.org/10.1109/IGARSS.2009.5417636.

Leuliette, E.W., Steven Nerem, R., Mitchum, G.T., 2004. Calibration of TOPEX/Poseidon and Jason altimeter data to construct a continuous record of mean sea level change. Mar. Geod. 27, 79–94. https://doi.org/10.1080/01490410490465193.

Long, C.S., Fujiwara, M., Davis, S., Mitchell, D.M., Wright, C.J., 2017. Climatology and interannual variability of dynamic variables in multiple reanalyses evaluated by the SPARC reanalysis intercomparison project (S-RIP). Atmos. Chem. Phys. 17 (23), 14593–14629.

Lorente, P., Sotillo, M.G., Aouf, L., Amo-Baladrón, A., Barrera, E., Dalphinet, A., Toledano, C., Rainaud, R., De Alfonso, M., Piedracoba, S., Basañez, A., García-Valdecasas, J.M., Pérez-Muñuzuri, V., Álvarez-Fanjul, E., 2018. Extreme wave height events in NW Spain: a combined multi-sensor and model approach. Remote Sens. 10, 1.

Łyszkowicz, A.B., Bernatowicz, A., 2017. Current state of art of satellite altimetry. Geod. Cartogr. 66, 259–270. https://doi.org/10.1515/geocart-2017-0016.

Madsen, K.S., Høyer, J.L., Fu, W., Donlon, C., 2015. Blending of satellite and tide gauge sea level observations and its assimilation in a storm surge model of the North Sea and Baltic Sea. J. Geophys. Res. Oceans 120, 6405–6418. https://doi.org/10.1002/2015JC011070.

Maiwald, F., et al., 2016. Reliable and stable radiometers for Jason-3. IEEE J. Select. Topics Appl. Earth Observ. Remote Sens. 9 (6), 2754–2762. June 2016. https://doi.org/10.1109/JSTARS.2016.2535281.

Maiwald, et al., 2020. Completion of the AMR-C instrument for sentinel-6. In: IEEE Journal of Selected Topics in Applied Earth Observations and Remote Sensing, vol. 13, pp. 1811–1818, 2020. https://doi.org/10.1109/JSTARS.2020.2991175.

Matevosyan, H., Lluch, I., Poghosyan, A., Golkar, A., 2017. A value-chain analysis for the Copernicus earth observation infrastructure evolution: a knowledgebase of users, needs, services, and products. IEEE Geosc. Remote Sens Magaz 5 (3), 19–35. Sept. 2017. https://doi.org/10.1109/MGRS.2017.2720263.

Ménard, Y., Fu, L.-L., 2001. Jason-1 Mission science plan, AVISO newsletter 8, AVISO altimetry edition, Ramonville St. Agne, France, 2001.

Mertikas, S.P., Ioannides, R.T., Tziavos, I.N., Vergos, G.S., Hausleitner, W., Frantzis, X., Tripolitsiotis, A., Partsinevelos, P., Andrikopoulos, D., 2010a. Statistical models and latest results in the determination of the absolute bias for the radar altimeters of Jason satellites using the Gavdos facility. Mar. Geod. 33 (1), 114–149. https://doi.org/10.1080/01490419.2010.488973.

Mertikas, S.P., Ioannides, R.T., Tziavos, I.N., Vergos, G.S., Hausleitner, W., Frantzis, X., Tripolitsiotis, A., Partsinevelos, P., Andrikopoulos, D., 2010b. Statistical models and latest results in the determination of the absolute bias for the radar altimeters of jason satellites using the gavdos facility. Mar. Geod. 33 (S1), 114–149, 2010b.

Mertikas, S.P., et al., 2010c. Statistical models and latest results in the determination of the absolute bias for the radar altimeters of Jason satellites using the Gavdos facility. Mar. Geod. (Suppl. 1), 114–149. https://doi.org/10.1080/01490419.2010.488973.

Mertikas, S.P., Daskalakis, A., Koutroulis, E.F., Tripolitsiotis, A., Partsinevelos, P., 2011. Preparatory works for the altimeter calibration of the Sentinel-3 mission using the dedicated calibration site in Crete and Gavdos. In: Proc. SPIE 8175, Remote Sensing of the Ocean, Sea Ice, Coastal Waters, and Large Water Regions 2011, 81750U (October 07, 2011). https://doi.org/10.1117/12.899133.

Mertikas, S., Donlon, C., Féménias, P., Mavrocordatos, C., Galanakis, D., Tripolitsiotis, A., Frantzis, X., Kokolakis, C., Tziavos, I.N., Vergos, G., Guinle, T., 2018. Fifteen years of Cal/Val service to reference altimetry missions: calibration of satellite altimetry at the permanent facilities in Gavdos and Crete, Greece. Remote

Sens. 10, 1557. https://doi.org/10.3390/rs10101557. https://www.mdpi.com/2 072-4292/10/10/1557.

Mertikas, S.P., Donlon, C., Cullen, R., Tripolitsiotis, A., 2019a. Scientific and Operational Roadmap for Fiducial Reference Measurements in Satellite Altimetry Calibration & Validation. International Association of Geodesy Symposia. Chap 61. https://doi. org/10.1007/1345_2019_61.

Mertikas, S.P., Donlon, C., Femenias, P., Cullen, R., Galanakis, D., Frantzis, X., Tripolitsiotis, A., 2019b. Fiducial Reference Measurements for Satellite Altimetry Calibration: The Constituents. International Association of Geodesy Symposia, Chap 56. https://doi.org/10.1007/1345_2019_56.

Mertikas, S, Tripolitsiotis, A, Donlon, C, Mavrocordatos, C, Fémenias, P, Borde, F, Frantzis, X, Kokolakis, C, Guinle, T, Vergos, G, Tziavos, I, Cullen, R, 2020. The ESA Permanent Facility for Altimetry Calibration: Monitoring Performance of Radar Altimeters for Sentinel-3A, Sentinel-3B and Jason-3 Using Transponder and Sea-Surface Calibrations with FRM Standards. Remote Sensing 12, 2642. https://doi. org/10.3390/rs12162642.

Mitchum, G., 1998. Monitoring the stability of satellite altimeters with tide gauges. J. Atmos. Ocean. Technol. 15, 721–730.

Moreau, T., Tran, N., Aublanc, J., Tison, L., Le Gac, S., Boy, F., 2018. Impact of long ocean waves on wave height retrieval from SAR altimetry data. Adv. Space Res. 62 (6), 1434–1444. https://doi.org/10.1016/j.asr.2018.06.004.

Munk, W., 2002. Testimony of Walter Munk to the U.S Commission on Ocean Policy, San Pedro, California 18 April 2002. available from. https://govinfo.library.unt.edu/oc eancommission/meetings/apr18_19_02/munk_statement.pdf.

NASA, 2011. OSTM End of Prime Mission Report, 2011. NASA Headquarters, Washington, DC, USA.

Nerem, R.S., Beckley, B.D., Fasullo, J.T., Hamlington, B.D., Masters, D., Mitchum, G.T., 2018. Climate-change–driven accelerated sea-level rise detected in the altimeter era. Proc. Natl. Acad. Sci. 115 (9), 2022–2025.

Nouël, F., Bardina, J., Jayles, C., Labrune, Y., Truong, B., 1988. DORIS: a precise satellite positioning Doppler system, Astrodynamics 1987. In: Soldner, J.K., Misra, A.K., Lindberg, R.E., Williamson, W. (Eds.), Adv Astron Sci, vol 65. American Astronautical Society, Springfield, pp. 311–320.

NRC, 2004. Climate Data Records from Environmental Satellites, Committee on Climate Data Records from NOAA Operational Satellites; Board on Atmospheric Sciences and Climate; Division on Earth and Life Studies; National Research Council, 150pp. ISBN: 978–0–309-09168-8. https://doi.org/10.17226/10944.

Parke, M.E., Stewart, R.H., Farless, D.L., Cartwright, D.E., 1987. On the choice of orbits for an altimetric satellite to study ocean circulation and tides. J. Geophys. Res. 92 (C11), 11693–11707. https://doi.org/10.1029/JC092iC11p11693.

Passaro, M., Cipollini, P., Vignudelli, S., Quartly, G.D., Snaith, H.M., 2014. ALES: A multi-mission adaptive subwaveform retracker for coastal and open ocean altimetry. Remote Sens. Environ. 145, 73–189. https://doi.org/10.1016/j.rse.2014.02.008.

Pavlis, C.E., Mertikas, S.P., the GAVDOS Team, 2004. The GAVDOS mean sea level and altimeter calibration facility: results for Jason-1. Mar. Geod. 27, 631–655.

Phalippou, L., Deemster, F., 2013. Ocean SAR altimetry from SIRAL2 on CryoSat2 to Poseidon-4 on Jason-CS, presented at the SAR Altimetry EGM, NOC, Southampton, united Kingdom, 26 June 2013.

Phalippou, L., Caubet, E., Deemster, F., Richard, J., Rys, L., Deschaux-Beaume, M., Francis, R., Cullen, R., 2012. Reaching sub-centimeter range noise on Jason-CS with the Poseidon-4 continuous SAR interleaved mode, Ocean Surface Topography Science Team 2012, Venice, Italy, 27–28 September 2012, available at. http://www. aviso.oceanobs.com/en/user-corner/science-teams/ostst-swt-science-team/ostst-2012-venice.html (last access: 24 March 2016). 2012.

Ponte, R.M., Carson, M., Cirano, M., Domingues, C.M., Jevrejeva, S., Marcos, M., Mitchum, G., van de Wal, R.S.W., Woodworth, P.L., Ablain, M., Ardhuin, F., Ballu, V., Becker, M., Benveniste, J., Birol, F., Bradshaw, E., Cazenave, A., De Mey-Frémaux, P., Durand, F., Ezer, T., Fu, L., Fukumori, I., Gordon, K., Gravelle, M., Griffies, S.M., Han, W., Hibbert, A., Hughes, C.W., Idier, D., Kourafalou, V., Little, C. M., Matthews, A., Melet, A., Merrifield, M., Meyssignac, B., Minobe, S., Penduff, T., Picot, N., Piecuch, C., Ray, R.C., Rickards, L., Santamaría-Gómez, A., Stammer, D., Staneva, J., Testut, L., Thompson, K., Thompson, P., Vignudelli, S., Williams, J., Williams, S.D.P., Wöppelmann, G., Zanna, L., Zhang, X., 2019. Towards comprehensive observing and modeling systems for monitoring and predicting regional to coastal sea level. Front. Mar. Sci. 6 https://doi.org/10.3389/ fmars.2019.00437, 437-.

Quartly, G.D., 2009. Improving the intercalibration of σ0 values for the Jason-1 and Jason-2 altimeters. IEEE Geosci. Rem. Sens. Lett. 6 (3), 538–542. https://doi.org/ 10.1109/LGRS.2009.2020921.

Quartly, G.D., Srokosz, M.A., Guymer, T.H., 1999. Global precipitation statistics from dual-frequency TOPEX altimetry. J. Geophys. Res. 104 (D24), 31489–31516. https://doi.org/10.1029/1999JD900758.

Quartly, G.D., Srokosz, M.A., Guymer, T.H., 2000. Changes in oceanic precipitation during the 1997–98 El Niño. Geophys. Res. Lett. 27 https://doi.org/10.1029/ 1999GL011311.

Quartly, G.D., Legeais, J.-F., Ablain, M., Zawadzki, L., Fernandes, M.J., Rudenko, S., Carrère, L., García, P.N., Cipollini, P., Andersen, O.B., Poisson, J.-C., Mbajon Njiche, S., Cazenave, A., Benveniste, J., 2017. A new phase in the production of quality-controlled sea level data. Earth Syst. Sci. Data 9, 557–572. https://doi.org/ 10.5194/essd-9-557-2017, 2017.

Quartly, G.D., Nencioli, F., Raynal, M., Bonnefond, P., Nilo Garcia, P., Garcia-Mondéjar, A., Flores de la Cruz, A., Crétaux, J.-F., Taburet, N., Frery, M.-L., Cancet, M., Muir, A., Brockley, D., McMillan, M., Abdalla, S., Fleury, S., Cadier, E., Gao, Q., Escorihuela, M.J., Roca, M., Bergé-Nguyen, M., Laurain, O., Bruniquel, J., Féménias, P., Lucas, B., 2020. The roles of the S3MPC: monitoring, validation and evolution of sentinel-3 altimetry observations. Remote Sens. 12, 1763.

Quilfen, Y., Chapron, B., 2019. Ocean surface wave-current signatures from satellite altimeter measurements. Geophys. Res. Lett. 46, 253–261. https://doi.org/10.1029/ 2018GL081029.

Raney, R.K., 1998. The delay/Doppler radar altimeter. IEEE Trans. Geosci. Rem. Sens. 36, 1578–1588. https://doi.org/10.1109/36.718861.

Ray, R.D., 2020. Daily harmonics of ionospheric total electron content from satellite altimetry. J. Atmos. Sol. Terr. Phys. 209, 105423. https://doi.org/10.1016/j. jastp.2020.105423.

Ray, C., et al., 2015. SAR altimeter backscattered waveform model. IEEE Trans. Geosci. Remote Sens. 53 (2), 911–919. Feb. 2015. https://doi.org/10.1109/TGRS.2014.233 0423.2020.

Reale, F., Pugliese Carratelli, E., Di Leo, A., Dentale, F., 2020. Wave orbital velocity effects on radar Doppler altimeter for sea monitoring. J. Mar. Sci. Eng. 8, 447.

Recchia, L., Scagliola, M., Giudici, D., Kuschnerus, M., 2017. An accurate semianalytical waveform model for mispointed SAR interferometric altimeters. IEEE Geosci. Remote Sens. Lett. 14 (9), 1537.

Ribal, A., Young, I.R., 2019. 33 years of globally calibrated wave height and wind speed data based on altimeter observations. Nat-Sci Data 6 (77), 1–15.

Roohi, Sh., Amini, A., Voosoghi, B., Battles, D., 2019. Lake monitoring from a combination of multi copernicus missions: sentinel-1 A and B and Sentinel3A. J Hydrogeol Hydrol Eng 8, 3.

Ruf, C., Keihm, S., Janssen, M.A., 1995. TOPEX/Poseidon microwave radiometer (TMR): I. instrument description and antenna temperature calibration. IEEE Trans. Geosci. Remote Sens. 33 (1), 125–137.

Sandwell, D.T., Harper, H., Tozer, B., Smith, W.H.F., 2019. Gravity field recovery from geodetic altimeter missions. Adv. Space Res. https://doi.org/10.1016/j. asr.2019.09.011.

Scharroo, R., 2018. Sentinel-6 end-user requirements document, EUM/LEO-JASCS/REQ/ 12/0013, v3E available from EUMETSAT. Darmstadt, Germany.

Scharroo, R., Lillibridge, J.L., Smith, W.H.F., Schrama, E.J.O., 2004. Cross-calibration and long-term monitoring of the microwave radiometers of ERS, TOPEX, GFO, Jason, and Envisat. Mar. Geod. 27 (1–2), 279–297. https://doi.org/10.1080/ 01490410490465265.

Scharroo, R., Smith, W.H.F., Lillibridge, J.L., 2005. Satellite altimetry and the intensification of Hurricane Katrina. Eos Trans. AGU 86 (40), 366. https://doi.org/ 10.1029/2005EO400004.

Scharroo, R., Leuliette, E.W., Lillibridge, J.L., Byrne, D., Naeije, M.C., Mitchum, G.T., 2013. RADS: consistent multi-mission products. In: Proc. of the Symposium on 20 Years of Progress in Radar Altimetry, Venice, 20-28 September 2012, Eur. Space Agency Spec. Publ., ESA SP-710, p. 4 pp, 2013.

Scharroo, R., Bonekamp, H., Ponsard, C., Parisot, F., von Engeln, A., Tahtadjiev, M., de Vriendt, K., Montagner, F., 2016. Jason continuity of services: continuing the Jason altimeter data records as Copernicus Sentinel-6. Ocean Sci. 12, 471–479. https://doi. org/10.5194/os-12-471-2016.

Scherllin-Pirscher, B., Steiner, A.K., Kirchengast, G., 2014. Deriving dynamics from GPS radio occultation: three-dimensional wind fields for monitoring the climate. Geophys. Res. Lett. 41 (20), 7367–7374.

Sibthorpe, A., Brown, S., Desai, S.D., Haines, B.J., 2011. Calibration and validation of the Jason-2/OSTM advanced microwave radiometer using terrestrial GPS stations. Mar. Geod. 34 (3–4), 420–430. https://doi.org/10.1080/01490419.2011.584839.

Smith, W.H., Sandwell, D.T., 1997. Global sea floor topography from satellite altimetry and ship depth soundings. Science 277, 1956–1962. https://doi.org/10.1126/ science.277.5334.1956.

Smith, W.H.F., Scharroo, R., Titov, V.V., Arcas, D., Arbic, B.K., 2005. Satellite altimeters measure tsunami. Oceanogray 18 (2), 11–13. https://doi.org/10.5670/ oceanog.2005.62.

Steunou, N., Desjonquères, J.D., Picot, N., Sengenes, P., Noubel, J., Poisson, J.C., 2015. AltiKa altimeter: instrument description and in flight performance. Mar. Geod. 38 (sup1), 22–42. https://doi.org/10.1080/01490419.2014.988835.

Taburet, N., Zawadzki, L., Vayre, M., Blumstein, D., Le Gac, S., Boy, F., Raynal, M., Labroue, S., Crétaux, J.-F., Femenias, P., 2020. S3MPC: improvement on inland water tracking and water level monitoring from the OLTC onboard sentinel-3 altimeters. Remote Sens. 2020 (12), 3055.

Tilling, R.L., Ridout, A., Shepherd, A., 2018. Estimating Arctic sea ice thickness and volume using CryoSat-2 radar altimeter data. Adv. Space Res. 62 (6), 1203–1225. https://doi.org/10.1016/j.asr.2017.10.051.

Tournadre, J., 2014. Anthropogenic pressure on the open ocean: the growth of ship traffic revealed by altimeter data analysis. Geophys. Res. Lett. 41, 7924–7932.

Tournadre, J., Whitmer, K., Girard-Ardhuin, F., 2008. Iceberg detection in open water by altimeter waveform analysis. J. Geophys. Res. 113, C08040 https://doi.org/ 10.1029/2007JC004587.

Tran, N., Vandemark, D., Ruf, C.S., Chapron, B., 2002. The dependence of nadir ocean surface emissivity on wind vector as measured by microwave radiometer. IEEE Trans. Geosci. Remote Sens. 40 (2), 515–523. Feb. 2002. https://doi.org/10.1109/ 36.992827.

Valladeau, G., Legeais, J.F., Ablain, M., Guinehut, S., Picot, N., 2012. Comparing altimetry with tide gauges and argo profiling floats for data quality assessment and mean sea level studies. Mar. Geod. 35 (sup1), 42–60. https://doi.org/10.1080/ 01490419.2012.718226.

Varma, A.K., Mangalsinh, N.R., Piyush, D.N., 2020. Precipitation measurement from SARAL AltiKa and passive microwave radiometer observations. Int. J. Remote Sens. 41 (23), 8948–8964. https://doi.org/10.1080/01431161.2020.1797214.

Vaze, P., Neeck, S., Bannoura, W., Green, J., Wade, A., Mignogno, M., Zaouche, G., Couderc, V., Thouvenot, E., Parisot, F., 2010. The Jason-3 Mission: completing the transition of ocean altimetry from research to operations. In: Proc. SPIE 7826,

Sensors, Systems, and Next-Generation Satellites XIV, 78260Y (13 October 2010). https://doi.org/10.1117/12.868543.

Veng, T., Andersen, O.B., 2020. Consolidating sea level acceleration estimates from satellite altimetry. Adv. Space Res. https://doi.org/10.1016/j.asr.2020.01.016.

Verkhoglyadova, O.P., Leroy, S.S., Ao, C.O., 2014. Estimation of winds from GPS radio occultations. J. Atmos. Ocean. Technol. 31 (11), 2451–2461.

Vignudelli, S., Kostianoy, A.G., Cipollini, P., Benveniste, J., 2011. Coastal Altimetry, 2011. Springer, ISBN 978-3-642-12795-3.

Walsh, E.J., 1982. Pulse-to-pulse correlation in satellite radar altimeters. Radio Sci. 17 (4), 786–800. https://doi.org/10.1029/RS017i004p00786.

Watson, C.S., White, N., Church, J., Burgette, R., Tregoning, P., Coleman, R., 2011. Absolute calibration in Bass Strait, Australia: TOPEX/Poseidon, Jason-1 and OSTM/ Jason-2. Mar. Geod. 34 (3–4), 242–260. https://doi.org/10.1080/01490419.2011.584834.

WCRP, 2018. Global Sea Level Budget Group (the), Global sea level budget, 1993-present. Earth System Science Data 10, 1551–1590. https://doi.org/10.5194/essd-10-1551-2018.

Wingham, D.J., Francis, C.R., Baker, S., Bouzinac, C., Brockley, D., Cullen, R., de Chateau-Thierry, P., Laxon, S.W., Mallow, U., Mavrocordatos, C., Phalippou, L., Ratier, G., Rey, L., Rostan, F., Viau, P., Wallis, D.W., 2006. CryoSat: a mission to determine the fluctuations in Earth's land and marine ice fields. Adv. Space Res. 37 (4), 841–871. https://doi.org/10.1016/j.asr.2005.07.027.

Zawadzki, L., Ablain, M., 2016. Accuracy of the mean sea level continuous record with future altimetric missions: Jason-3 vs. sentinel-3a. Ocean Sci. 12, 9–18, 2016.